

# Emerging Trends in Engineering and Technology

Volume - 3

**Chief Editor**

**Mohit Bajpai**

Associate Professor, Electronics and Communication Engineering, Poornima  
Institute of Engineering & Technology, Jaipur, Rajasthan, India

**Co-Editor**

**Dr. A.V. Sudhakara Reddy**

Associate Professor, R&D Coordinator, Department of Electrical and  
Electronics Engineering, Malla Reddy Engineering College (Autonomous),  
Maisammaguda, Secunderabad, Telangana, India

**Dr. Rajesh Reddy. Duvvuru**

Assistant Professor, Department of Electrical & Electronics Engineering,  
Narayana Engineering College (A), Gudur, Andhra Pradesh, India

**Integrated Publications  
New Delhi**

**Published By:** Integrated Publications

Integrated Publications

H. No. - 3 Pocket - H34, Sector - 3,

Rohini, Delhi-110085, India

**Chief Editor:** Mohit Bajpai

The author/publisher has attempted to trace and acknowledge the materials reproduced in this publication and apologize if permission and acknowledgements to publish in this form have not been given. If any material has not been acknowledged please write and let us know so that we may rectify it.

© **Integrated Publications**

**Publication Year:** 2021

**Pages:** 86

**ISBN:** 978-93-90471-76-8

**Book DOI:** <https://doi.org/10.22271/int.book.89>

**Price:** ₹ 796/-

# Contents

<b>S. No.</b>	<b>Chapters</b>	<b>Page No.</b>
1.	A Novel Convolution Neural Network Based Real Time Object Detection and Identification for Video Surveillance Systems <i>(Rajesh Reddy Duvvuru, N. Bhargavi and Raja Reddy Duvvuru)</i>	01-15
2.	Discrete Wavelet Transform (DWT) Based Image Watermarking <i>(A. Hazarthaiah, Ch. Narendra Kumar and D. Saritha)</i>	17-27
3.	Solar Photo-Fenton Degradation of Trypan Blue Dye in Wastewater: Batch Kinetic Study <i>(P. Shanthi Priya and P. Neha)</i>	29-41
4.	Analysis of Digital Image Based on CT Scans <i>(B. Mala Konda Reddy, Rajesh Reddy Duvvuru and Ch. Narendra Kumar)</i>	43-52
5.	Performance of Modal Analysis and Finite Element Analysis <i>(S.C. Sireesha and D. Lakshmi Sravanthi)</i>	53-63
6.	Assessment of Real Time ID using RFID <i>(P. Sree Lak, Raja Reddy Duvvuru and D. Saritha)</i>	65-76
7.	Design Analysis of Ultra-Wide Band Micro Strip Patch Antenna <i>(M.V.S. Sudheer Babu, M. Kondalu and Rajesh Reddy Duvvuru)</i>	77-86



**Chapter - 1**  
**A Novel Convolution Neural Network Based Real  
Time Object Detection and Identification for  
Video Surveillance Systems**

**Authors**

**Rajesh Reddy Duvvuru**

Department of Electrical & Electronics Engineering, Narayana  
Engineering College, Gudur, Andhra Pradesh, India

**N. Bhargavi**

Department of Electronics and Communication Engineering,  
Audisankara Institute of Technology, Gudur, Andhra Pradesh,  
India

**Raja Reddy Duvvuru**

Department of Electrical & Electronics Engineering, Malla  
Reddy Engineering College (Autonomous), Hyderabad,  
Telangana, India



# Chapter - 1

## A Novel Convolution Neural Network Based Real Time Object Detection and Identification for Video Surveillance Systems

Rajesh Reddy Duvvuru, N. Bhargavi and Raja Reddy Duvvuru

### Abstract

In this paper, Recognition and tracking of the object is one of the critical challenges that many of the existing works are focusing on. Mainly the detection of object and tracking is very much popular because of the growing demands in the video surveillance system applications like traffic controlling, medical image processing and satellite image processing applications. This is also of the most powerful algorithms in the field of computer vision, machine learning, Artificial Intelligence based applications. The ultimate objective of these underlying object recognition-based systems is to comprehend the type of images, characteristics, location of the each images in the space and the tracking the movements of each objects while moving. Many objects detection applications used for detection of objects are mainly concentrating on identification of human as it has got lot of attention in the existing research works.

This section describes a new approach to recognizing objects using the CNN approach for the detection of the non-living objects as well as human objects. The main objective of this section is providing a framework that can be able to identify both the type of objects like living and non-living. Once they are identified they can be classified and using support vector machine technique, this will be helpful for the theft identification using the surveillance systems.

**Keywords:** CNN, Image processing, SVM

### I. Introduction

In modern Object recognition is one of the main challenges facing most computer vision work. Increasing demands on surveillance, security, traffic management and medical imaging are particularly popular in object detection and tracking <sup>[1]</sup>. It is also a product of strong algorithms in machine

learning, computer vision and hardware advances that enable a couple of minutes of highly data-intensive calculations. The ultimate aim of the vision-based detection is to understand the type of objects in the picture, their characteristics and their location in the space and to move or track the object.

Image Processing is the field where various number of research work has been taken up and implemented successfully. With increasing concerns for public safety and security nowadays, the need for automatic surveillance systems based on real time videos of public places is realized. The highly crowded and sensitive places like markets, shopping space, famous restaurants, railway stations etc. Must be equipped with these surveillance systems. Without constraining their application to security under public spaces, they are also most demanded for the purposes of traffic control and examination, activity recognition and tracking, fault detection in industrial applications and semantic video indexing. In order to achieve the high-level tasks of classification or tracking a target from video stream, the strategy used is to detect the target of interest in individual frames in the first place [7].

The technique used in many of the works for surveillance is the Background subtraction method. This technique performs extraction of the foreground object i.e. the target under motion by separating the background and foreground pixels in the frame under processing. The advantages of this method namely the performance in the presence of a non-mobile video camera and illumination invariance are well exploited by many researchers. The building of a background model of the captured video frame is a key point to be considered. For feature extraction for detection of objects, textures such as Local Pattern Binary (LBP) [2] of the image have been considered. Pixel neighbourhood operations are used to compute LBP characteristics. Histogram of oriented gradients is a common feature descriptor for object detection. HOG features are shape descriptors that represent an object in specific directions in terms of intensity gradients. In [3], the researchers took advantage of HOG [4] functions, citing their invariance properties in regard to transformations such as rotation, deformities and conditions of illumination.

## **II. System design for the proposed method**

The system design phase provides an abstract representation for the proposed research work which describes the complete flow of the research work how each module has to be implemented and integrated by the efficient application development.

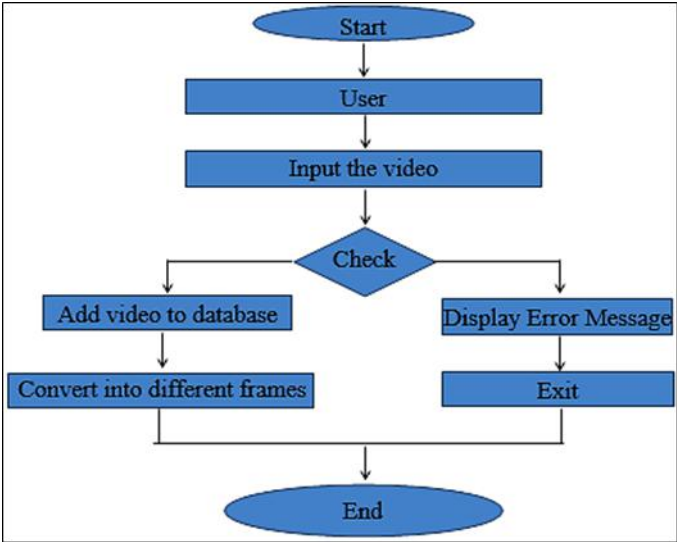


**Design diagram-high level**

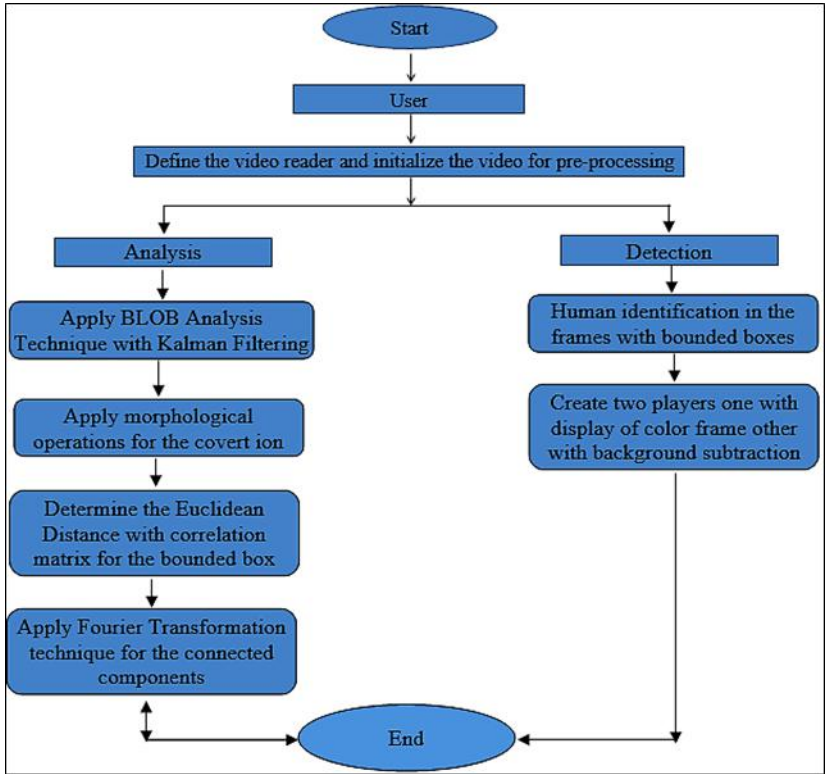
This design diagram describes the representation of all the modules in the proposed technique and provides solution for the services offered by the system to produce the high-quality design for the research work. In a multi-project model, such an outline is important to ensure that each supporting element design is consistent with the neighboring designs and the large picture. All the services of the proposed system, the platform used and the process of implementation should be described in the brief manner and any important change needed to be done and integrated to be specified in this stage. Furthermore, all major commercial, legal, environmental, safety and safety matters should be considered briefly.

**Design diagram-high level**

This diagram presents in the form of bubble graphs can be defined as dfds. Data flow diagram is one of the easiest graphical representations describes in figure 1 & 2 <sup>[8]</sup>.



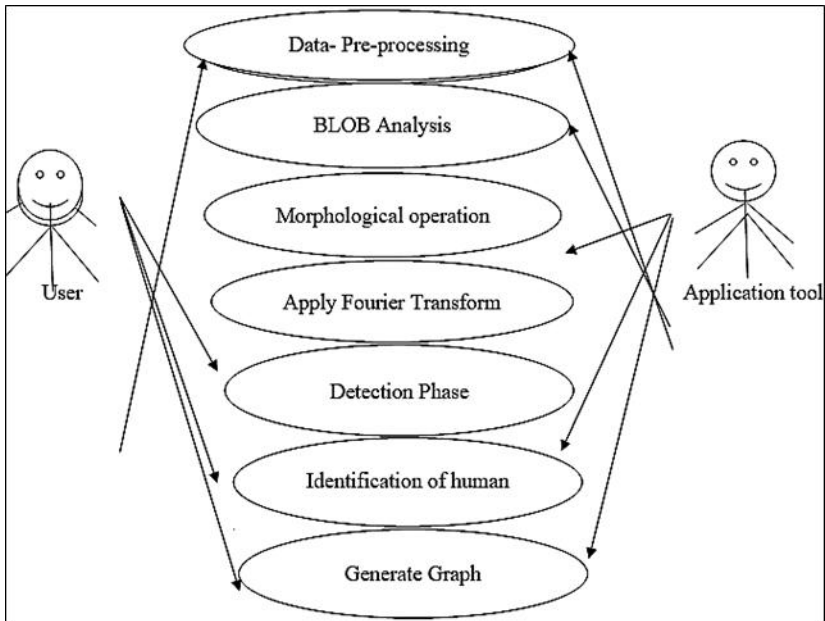
**Fig 1:** Data Flow Diagram for Add Database



**Fig 2:** Data Flow Diagram for Proposed Technique

### Case diagram

Case diagram depicted in below figure. 3 describes the communication between the end user and the application framework; the functionality for the communication will be recorded and performed accordingly.



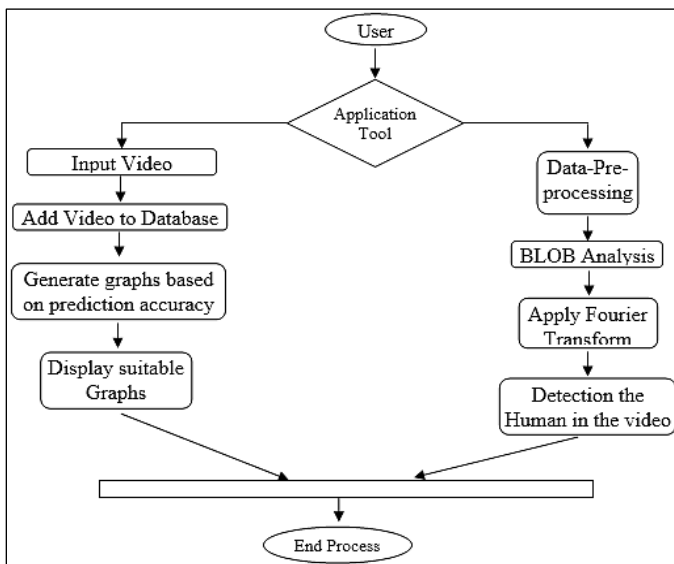
**Fig 3:** The Use case diagram for Proposed Technique

The characters who are involved in the process will be referred as on-screen characters and who are performing outside the framework will be referred as performing artists. The main objective of this design diagram is to describe how the communication between each module is done, that's helps in the implementation of the work.

### **Design diagram-activity**

The activity diagram describes in the figure. 4, presents the important activities carried out in the research work. In this diagram the circles represents the start of the activity and the end of an activity and the rectangle boxes defines the modules of each proposed research work <sup>[9]</sup>.

The purpose of activity diagram in the proposed framework is to make sure the workflow of the application development is implemented according to the desired requirements provided by the end users. The developer will refer these design diagrams for the implementation of the work.



**Fig 4:** The activity diagram for Proposed Technique

### III. Process of identification of objects and the classification technique

**Step 1:** Input the video that contains both human and non-living moving objects.

**Step 2:** Pre-processing the input video: The input video to be pre-processed is two different steps:

- Divide the input video into frames and store individually.
- Once frames are generated apply the morphological operations over the input video.

#### Image pre-processing and annotation

Image Pre-Processing involves processing or cleaning of images. This step focuses on removal of noise and distortion, sharpening, intensity normalization, etc. The VOC dataset is refined with only person images and annotated according to the format of YOLO model. A text file is created for each image in the same directory with the same name that contains object number and object coordinates on this image, for each object in new line. The object numbers an integer number of object from zero to total number of classes-1, and object coordinates are float values relative to width and height of image, it can be equal from (0.0 to 1.0]. The ID card images are only pre-processed <sup>[10]</sup>.

## Training the YOLO model and testing

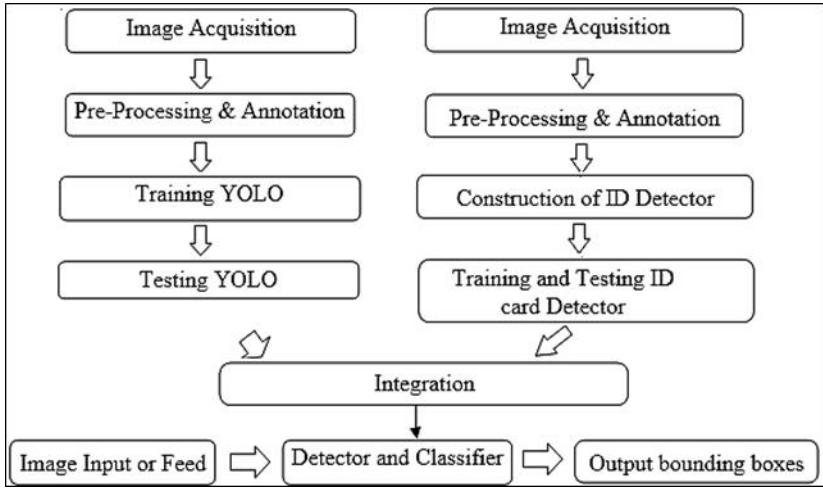
After pre-processing and annotation, the person dataset is divided into training and testing datasets. We train the YOLO model using training dataset until we get a better mean Average Precision (map). After the training, it is tested with testing dataset. YOLO is a full convolution network consisting built using darknet-53. It detects objects at three different strides (8, 16 and 32) which help to detect smaller objects. The provided input image will be divided into  $S \times S$  grid and each of the cell will be made of the coordinated of  $(x, y, w, h)$  and the confidence of the object. The representation of the coordinates  $x, y$  defines the position of the boundary box which is relatively grid in nature. The coordinates with  $w, h$  is represented as the width and height of the detected boundary box. The probability of each grid is predicted for  $C$  categories. The confidence is determined by the probability model that includes the target and the prediction detection box. The object is defined as  $Pr$  which stands for the target object that falling under the cell. If the confidence is presents then it is defined using:

$$C(\text{Object}) = Pr(\text{Object}) * IOU(\text{Prod}, \text{Truth}) \quad (1)$$

The cell doesn't contain any kind of the object and the confidence values is defined as  $C(\text{object}) = 0$ . The IOU is defined as the overlapping rate for which the bound of candidate and the truth value of the ground can be defined as the ration of union and the intersection of the grounds <sup>[11-13]</sup>.

Then the classification of the objects is achieved by classifying them into their respective categories. Here, multi class SVM classification is used by supervised learning for the output of the object class.

The quality of CNN classification is determined over video data set checking: The category output is the class to which an object is identified. In a single frame, a vector containing all classes detected is generated as an output for multiple objects of different lasses.



**Fig 5:** System Architecture of proposed Framework

#### IV. Extraction of features for the identification of non-living objects

This section presents the detailed study of how the extraction of features has been implemented and the mathematical model related to the techniques used for feature extraction technique used will be described.

##### Corner detector using shi-tomasi technique

The Harris Corner Detector is an experimental model that detects the corner features from the video frames that provides higher texture features with minimal propositional changes. The harries technique is mainly used to detect the corners of the frames and it is carried out as follows:

The intensity of the pixel proposition is defined in  $I(x, y)$  for the position  $(x, y)$  of each window frame of the input video, and if the window moves by small margin the shift  $(e, v)$ , will be marked with  $I(x+u, y+v)$ . Since the main objective is to locate regions or windows with small displacements in the image, the intensity is expressed mathematically

$$E(u, v) = \sum_{x,y} w(x, y) [I(x + u, y + v) - I(x, y)]^2 \quad \dots (1)$$

The weight function is defined with 'W' and the high intensity variation in the window frames may lead to the result of  $E(u, v)$ .

The Taylor's series and simplification technique of Equation 1, provides the results in,

$$M = \sum w(x, y) \begin{bmatrix} I_x^2 & I_x I_y \\ I_x I_y & I_y^2 \end{bmatrix} \quad \dots (2)$$

The Eigen values of matrix is defined as M is used to find out suitable corners sing the score value,

$$S = |M| - k(\text{trace}(M))^2 \quad \dots (3)$$

If  $\lambda_1, \lambda_2$  Are Eigen values of M, then  $|M| = \lambda_1 \lambda_2$  and  $\text{trace}(M) = \lambda_1 + \lambda_2$

Each corners of the frame is represented using S, to predict the high score value. The smaller change in the calculation is calculated using the Shi-Tomasitechnique, that leads to the determining the most suitable corner defined in ‘n’, rather than identifying the each and every corner of the feature <sup>[14]</sup>.

Shi-Tomasi score for corner detection follows-

$$S = \min(\lambda_1, \lambda_2) \quad \dots (4)$$

If the score, S exceeds a threshold it is considered as a corner <sup>[9]</sup>.

### Determining the optimal flow using lucas-kanade technique

The optical flow of the detected fame has to be determined, that track the movement of the objects in frame when the object is moving or during the rotation of the camera. The optical flow of any kind of entity from one frame to another frame in a video is to be determined. The proposed algorithm Lucas-Kanade <sup>[5]</sup> is mainly based on the type of optical flow theory, where all the video frames remain in the similar kind of intensity and the pixels in the frames have similar kind of movements and the pixels rate between successive each frames smaller in nature.

A pixel rate <sup>[6]</sup> with the intensity rate defined as  $I(x,y,t)$  in a frame at time interval defined as  $t$  after the movement with a small displacement defined as  $(d_x, d_y)$  in the consecutive frames with a difference of time  $d_t$  Is expresses as:

$$I(x, y, t) = I(x + d_x, y + d_y, t + d_t) \quad \dots (5)$$

The flow of an optimal equation for the movement of objects in an image is given as-

$$\frac{\partial f}{\partial x} \frac{d_x}{d_t} + \frac{\partial f}{\partial y} \frac{d_y}{d_t} + f_t = 0 \quad \dots (6)$$

The optical flow motion of the vectors using Lucas-Kanade method is defined by solving Equation (6):

$$\begin{bmatrix} u \\ v \end{bmatrix} = \Sigma_{\square} \begin{bmatrix} f_{x_i}^2 & f_{x_i} f_{y_i} \\ f_{x_i} f_{y_i} & f_{y_i}^2 \end{bmatrix}^{-1} \Sigma_i \begin{bmatrix} -f_{x_i} f_{t_i} \\ -f_{y_i} f_{t_i} \end{bmatrix} \quad \dots (7)$$

The representation of the displacement defined  $I(u, v)$  represents the of the object between consecutive frames.

### V. Results and Discussions

The framework can be integrated within the Matlab tool kit that makes it possible to use its toolboxes for the computer vision and machine learning to easily integrate mathematical computations for the identification and classification of artifacts.

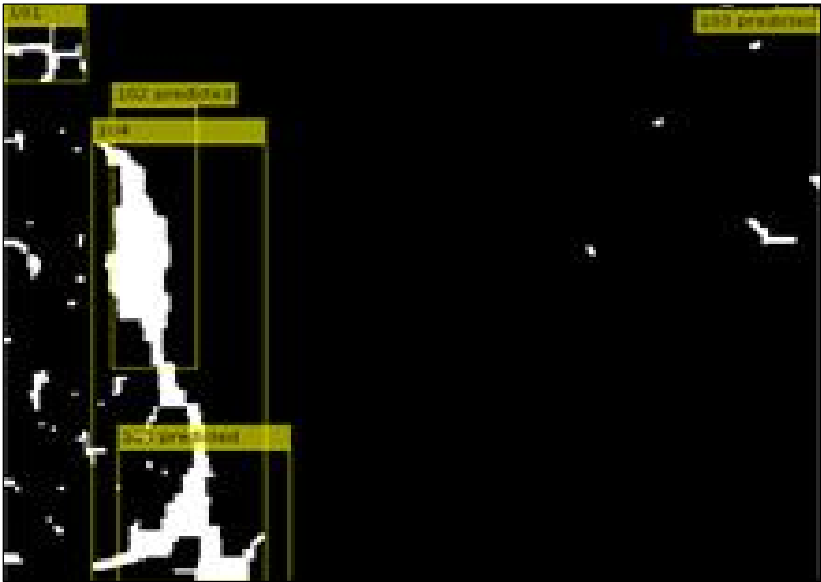
After extraction, the video processing is carried out smoothly on each frame. The toolbox for image processing includes several filtering and refining functions required to process an identified image before processing. A maximum of 15 videos containing standard products of various classes are collected. The dataset has been divided into three groups-5 video training datasets and 8 video test data sets required for vector support machine technique [15].

Figure 6 below shows the histogram of frames extracted from video 1 in which different objects are recognized in the same way after extracting characteristics, as in Figure 7 and Figure 8 various objects detected from video 6 and video 7 respectively.



**Fig 6:** Frame extraction for the detected objects in the inputvideo1





**Fig 7:** Frame extraction for the detected objects in the input video 2



**Fig 8:** Frame extraction for the detected objects in the input video 3

The final results are drawn using the proposed CNN framework where the input is given to the framework that contains both human and non-living objects in the video dataset. The input video will be processed and detects

the background and fore-ground of the objects. Initially pre-processing is applied to remove noise in the video and then morphological operations are applied to analyze the color pixel of the detected frames.

## **VI. Conclusion**

This work presented a new approach for object recognition using Vector Machine based classification in Video Surveillance Systems and Lucas-Kanade technique. In this article, the artifacts are correctly identified and their position from an unknown location is calculated. First, object recognition using Shi-Tomasi and Lucas-Kanade techniques will be stored, and the context subtraction will be applied when an object from extracted frames of the input video is recognized. Then the classification of the objects in their individual categories is accomplished by supervised learning with the help vector machine classification.

The precision of the technique being proposed is analyzed by the total number of frames detected by object compared to the total number of frames. In this chart four input videos from different sources of various sizes and backgrounds were taken, and for each video we should achieve 92 percent accuracy. Where frames vary from 500 to 1500 for each video, the exactness of the identification of the objects is 80 to 95% for each video.

## **References**

1. Pillai CS, Ananda Babu J. Object Recognition using Lucas-Kanade Technique and Support Vector Machine Based Classification in Video Surveillance Systems, *International Journal of Engineering and Advanced Technology (IJEAT)*, 2019, 9(1). ISSN:2249-8958.
2. Elliott D. Intelligent video solution: A definition, *Security*, 2010, 46-48.
3. Avidan S. Ensemble tracking, *IEEE Trans. Pattern Anal. Mach. Intell.* 2007; 29(2):261-271.
4. Kushwaha A, Sharma C, Khare M, Srivastava R, Khare A. Automatic multiple human detection and tracking for visual surveillance system. *International Conference on Informatics, Electronics Vision (ICIEV)*, 2012, 326-331.
5. Lucas BD, Kanade T. An iterative image registration technique with an application to stereo vision, in *IJCAI*, 1981.
6. Everingham M, Van Gool L, Williams CK, Winn J, Zisserman A. The Pascal Visual Object Classes (VOC) Challenge, *IJCV*, 2010, 30.

7. Avidan S. Ensemble tracking, *IEEE Trans. Pattern Anal. Mach. Intell.* 2007; 29(2):261-271.
8. Khan Z, Gu I. Joint feature correspondences and appearance similarity for robust visual object tracking, *IEEE Trans. Inf. Forensics Security.* 2010; 5(3):591-606.
9. Dalal N, Triggs B. Histograms of oriented gradients for human detection, in *Proc. CVPR*, 2005, 886-893.
10. Wang L. Abnormal walking gait analysis using silhouette-masked flow histograms, in *Proc. ICPR*. 2006; 3:473-476.
11. Wang S, Lee H. A cascade framework for a real-time statistical plate recognition system, *IEEE Trans. Inf. Forensics Security.* 2007; 2(2):267-282.
12. Yu X, Chinomi K, Koshimizu T, Nitta N, Ito Y, Babaguchi N. Privacy protecting visual processing for secure video surveillance, in *Proc. ICIP*, 2008, 1672-1675.
13. Park U, Jain A. Face matching and retrieval using soft biometrics, *IEEE Trans. Inf. Forensics Security.* 2010; 5(3):406-415.
14. Cong Y, Yuan J, Luo J. Towards scalable summarization of consumer videos via sparse dictionary selection, *IEEE Trans. Multimedia.* 2012; 14(1):66-75.
15. Cong Y, Gong H, Zhu S, Tang Y. Flow mosaicking: Real-time pedestrian counting without scene-specific learning, in *Proc. CVPR*, 2009, 1093-1100.



**Chapter - 2**  
**Discrete Wavelet Transform (DWT) Based Image**  
**Watermarking**

**Authors**

**A. Hazarthaiah**

Professor, Department of ECE, Narayana Engineering College,  
Gudur, Andhra Pradesh, India

**Ch. Narendra Kumar**

Associate Professor, Department of EEE, Malla Reddy  
Engineering College (A), Hyderabad, Telangana, India

**D. Saritha**

Assistant Professor, Department of CSE, Narayana Engineering  
College, Gudur, Andhra Pradesh, India



# Chapter - 2

## Discrete Wavelet Transform (DWT) Based Image Watermarking

A. Hazarthaiah, Ch. Narendra Kumar and D. Saritha

### Abstract

Digital image watermarking requires the embedded watermark to be resilient and retrievable even if the watermarked content undergoes one or more image processing operations, in part or as a whole. Consequently, it is proposed to evolve the watermark embedding strategy to satisfy the conflicting objectives of causing image content changes that are imperceptible to the human eye while being extremely robust against intentional and unintentional image processing attacks. It is assumed that the attacker knows the algorithm and so, the performance and security depend on the algorithm itself and the key(s) used. The attacker is expected to exploit the specific weakness of the algorithm to defeat the watermarking.

**Keywords:** DWT, SWD, HSV

### 1. Introduction

This chapter presents another robust watermarking technique based on Discrete Wavelet Transform (DWT) and Singular Value Decomposition (SVD) for color images using multiple watermarks. Like the other proposed techniques presented in Chapter 5 and 6, the cover images are used in Hue, Saturation and Value (HSV) color model. The Value plane (V-plane) is used for watermarking because changes in V-plane does not affect the color information and hence the changes are less visible. V-plane undergoes DWT to distribute the frequencies present in the cover image. As discussed in Chapter 3, the most suitable choice of frequency band for embedding the watermark are mid-frequency bands. The mid-frequency bands undergo SVD and the singular values obtained are used to hide watermark. The proposed work does not require the original watermark to be used for its extraction from the watermarked image and proves to be robust against general image processing attacks and ambiguity attacks. Optimization refers to finding the best choice for some function subject to specified conditions

that represent a range of available choices. Different methods of optimization have been used for image watermarking, for example, Genetic Algorithm (Bassel, Nordin, & Abdulkareem, 2017), Artificial Bee Colony (ABC) optimization (Ansari, Pant, & Ahn, 2016a), (Ansari, Pant, & Ahn, 2016c), Particle Swarm Optimization (PSO) (Tsai, Jhuang, & Lai, 2012), Firefly Algorithms (Mishra, Agarwal, Sharma, & Bedi, 2014) etc. Mostly, optimization has been used on strength factor to achieve highest possible imperceptibility and robustness. (Golshan & Mohammadi, 2014) used genetic algorithm to optimally select the best suitable watermark. Unlike optimizing the strength factor, this work uses optimization on singular values directly subject to maximizing Peak Signal to Noise Ratio (PSNR) to present a robust, blind watermarking technique for color images based on Singular Value Decomposition (SVD) of Discrete Wavelet Transform (DWT) coefficients. The cover image is read in Hue, Saturation and Value (HSV) color space and chromaticity information is preserved while V-plane is used for watermark embedding. The V-plane undergoes 2-level DWT to represent the data in seven frequency bands. Watermark is embedded in horizontal (HL) and vertical (LH) sub-bands of 2-level DWT. Each of these sub-bands is divided into non-overlapping blocks of size  $4 \times 4$ . For each block, SVD is performed and the singular values are updated based on watermark bit using Lagrange's optimization principle. Two keys are used during the embedding process. One of the keys is used to distribute watermark randomly for embedding in two sub-bands. Another key is used as a quantization step size during optimization of the singular values for watermark embedding.

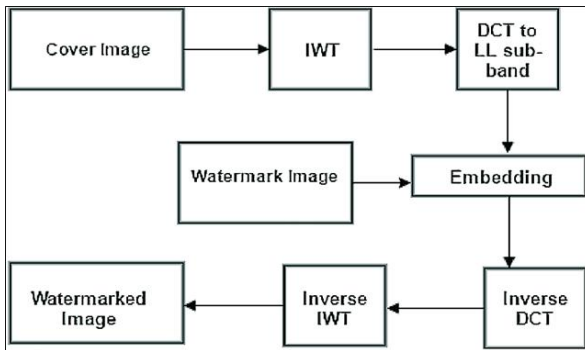
## **2. Image processing technique**

This section describes the embedding and extraction process of the proposed a blind method for color image watermarking in transform domain. The proposed method uses optimization of singular values to embed binary logo, hence is called Watermarking with Optimum Singular Values (WOSV). Applying optimization on the singular values directly eliminates the need of strength factor. Moreover, unlike the previously proposed method, Authentication-based Watermarking using Digital Signatures (AWDS), rather than embedding two copies of some data, the watermark,  $W$  is pre-processed and divided into two equal parts  $W_1$  and  $W_2$ , each to this section describes the steps of embedding and extraction of multiple watermarks into color images. The method uses DWT to identify frequency coefficients of the cover image to hide the watermarks. HL and LH frequency bands from DWT undergo SVD to update the singular values for hiding the watermark information and generate the keys. The presented



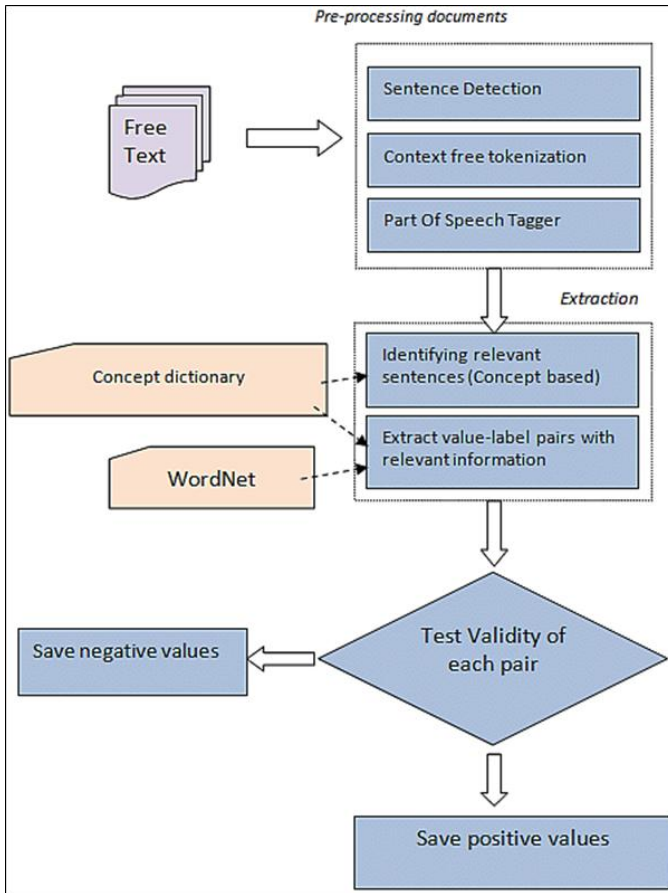
technique does not require any information about the watermark during extraction and relies on combination of keys rather than a single key which are generated based on the cover and watermark image. Hence the technique is called Cover Dependent Image Watermarking (CDIW). Any other processed version of the original cover will not be able to generate the correct keys for extraction. Instead of embedding watermark directly, its Principal Components (PCs) are embedded which are obtained using SVD of the watermark.

The proposed watermark embedding procedure uses two independent watermarks  $W1$  and  $W2$  to be embedded into cover image  $C$ , with a strength factors  $sf1$  and  $sf2$  respectively. Different approaches for hiding watermark is discussed which proved that updating the singular values of the cover image with weighted singular values of the watermark produced the highest imperceptibility. Hence, CDIW uses the same approach except that the singular.



**Fig 1:** Block diagram for embedding steps using CDIW

For a fake watermark claim, the reconstructed watermarks obtained in equations will display low correlation and similarity with the claimed watermarks. This prevents any false claim of watermarks and hence the technique offers robustness against false positives. The tests to prove the claim are conducted and their results are discussed in sections to follow. For the results presented for CDIW, the used cover image and the watermarks are shown in Fig. 1. The cover is a color image of baboon of size  $512 \times 512$  and the watermarks are grayscale images of a cameraman and a girl of size  $64 \times 64$ . The cameraman image is embedded in the HL band and the girl image is embedded in LH band for the experiments performed in later part of the chapter. To embed these watermarks into DWT coefficients, 3-level DWT is performed to obtain the HL and LH bands of the same size as watermarks.



**Fig 2:** Process flow diagram for extraction steps using CDIW

### 3. Proposed technique

The proposed technique is firstly tested against claims of false cover image. These false images may be any other uncorrelated image or some processed version of the original cover. As the coefficients from the original cover are required for reconstruction of the watermarks. Suppose that some malicious attacker uses another preprocessed version of the cover,  $C'$  during extraction to claim that the original cover was  $C'$  and not  $C$ . This is referred to as false cover claim.

The proposed technique can reject any such claim for cover image due to use of keys generated by combination of the original cover and watermarks during watermarking process. If these keys are generated by any other processed version of the original cover image,  $C$  the watermark will

not be extracted. The claimed covers are assumed to be some processed versions of the original and the claimed watermarks are same as the original watermarks. V-planes of the claimed covers with Normalized Correlation (NC) coefficient with respect to the V-plane of the original cover to present the results against false cover claim for CDIW approach.



**Fig 3:** Watermark images

For each of the claimed cover, the four secret keys are generated and their similarity to the corresponding original keys is displayed in terms of NC coefficient in for each of the processed version of the original cover image, it is observed that the NC coefficient between the original keys and the generated ones is quite small which indicates low similarity. Using these keys, approximate singular values are calculated for the final extraction of the watermarks. The NC coefficients of these approximate singular values of the two watermarks are also shown in second column of as NCASV1 and NCASV2.

As presented in there are many measures for imperceptibility and robustness of a watermarking technique. This section analyses the proposed work with respect to these measures, PSNR, Bit Correct Ratio (BCR), Bit Error Rate (BER), Structural Similarity Index Measure (SSIM) and Normalized Correlation (NC) coefficient. The proposed method is analysed using different binary watermark images of size 32×64 pixels, as shown in Fig.



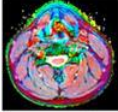





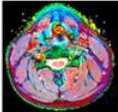





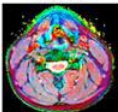





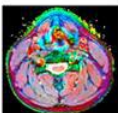





**Fig 4:** Cover images for different models

The first experiment is carried out with Lena as the cover image and Logo 1 as the watermark from Fig. 4 and Fig. 5 respectively it shows the variation in PSNR and SSIM between the original cover and the watermarked image with changes in quantization step size. The quantization step size is identified as key2 for the proposed WOSV method of blind watermarking. PSNR measured (in dB) and SSIM between the watermarked image and the original cover represent a measure of imperceptibility for the embedding technique. It is observed that with increasing quantization step size, PSNR decreases because of increasing quantization error which results in higher MSE. Also, SSIM between these images reduces showing that dissimilarity between the original and watermarked image increases due to more noise introduced due to a larger quantization steps.


















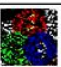
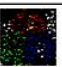

#### **4. Results**

The proposed OWSV technique shows promising results for watermarking colour images. The technique is imperceptible and robust against major image processing operations. However, this is achieved at the cost of smaller watermarks. Since there is no requirement of the originals at the time of extraction, the technique can resist false positive watermark extraction. The false negative rate is 0 with a precision of 88.23%. The execution time taken by the method for watermark embedding and extraction are 1.451084 seconds and 0.348125 seconds respectively. Additional security is provided by the keys used during embedding and extraction. Without using the actual keys, the watermark is not extracted successfully.

Methods	Single Watermarking					
	Lena Image		Medical Image		Military Image	
	PSNR (dB)	NC	PSNR (dB)	NC	PSNR (dB)	NC
original image + watermark	 41.7268	 0.9675	 41.7166	 0.9675	 41.7528	 0.9674
(original image with DWT) + watermark	 50.9085	 0.6586	 50.9005	 0.6586	 50.9096	 0.6586
(original image with SVD) + (watermark with SVD)	 42.1390	 1.00	 42.0294	 1	 42.1618	 1
(original image with DWT and SVD) + (watermark with SVD)	 44.3211	 1	 44.3427	 1	 44.6307	 1

**Fig 5:** Extracted watermarks for each of the cover images

A robust and secure watermarking method is presented in this chapter for color images. These images are used in HSV color model and its Value plane is used for embedding two different watermarks using DWT and SVD. Unlike AWDS, PCs of the two watermarks are obtained and embedded into singular values of the selective DWT coefficients of the cover image. The work proposed in this chapter, CDIW is proved to be robust against general image processing as well as ambiguity attacks too. Keys based on cover and watermarks are generated and used for cover and watermark verification during extraction. Hence the proposed technique is named as cover dependent watermarking. The claim of ownership of the watermarked image with a false or processed cover image is rejected. Also, fake watermark extraction is rejected since the extracted PCs combine with the original watermark coefficients only to produce a meaningful watermark. Coefficients of a fake watermark fail to prove ownership when combined with the extracted data from the watermarked image.

			
5% (NC = 1.0)	10% (NC = 1.0)	15% (NC = 1.0)	20% (NC = 0.9998)
			
25% (NC = 0.9994)	30% (NC = 0.9986)	35% (NC = 0.9971)	40% (NC = 0.9940)
			
45% (NC = 0.9913)	50% (NC = 0.9817)	55% (NC = 0.9741)	60% (NC = 0.9630)
			
65% (NC = 0.9429)	70% (NC = 0.9142)	75% (NC = 0.8779)	80% (NC = 0.8423)
			
85% (NC = 0.7855)	90% (NC = 0.6776)	95% (NC = 0.4568)	100% (NC = 0.0)

**Fig 6:** Extracted Watermarks after Image Processing Attacks

## Conclusion

The focus of the review is on transform domain watermarking with more focus on use of singular Value Decomposition (SVD) and Discrete Wavelet Transform (DWT), followed by mathematical study of the two transforms. The ambiguity issues with SVD are discussed and analysed for possible solutions. The next section of the chapter presents different performance measures available to evaluate the proposed watermarking techniques. The chapter also presents an overview of different colour spaces for image representation and identifies the advantages of using the HSV colour space for watermarking in the proposed works. The chapter concludes with identification of research gaps which forms the basis for the work proposed. The contribution of this research work starts from, a non-blind, hybrid transform domain method for colour image watermarking is explained which uses digital signatures to ensure that the proposed non-blind watermarking technique can resist any ambiguity in the claim of original watermark. The second proposed technique is explained.

## References

1. Askari MS, Javanshir AH. Investigating the Efficiency and Promotion of Watermarking based on Decomposition of Singular Values. International Journal of Computer Science and Network Security. 2017; 17(6):229-240.
2. Bassel A, Nordin MJ, Abdulkareem MB. An Improved Robust Image Watermarking Scheme based on the Singular Value Decomposition and

- Genetic Algorithm. *Advances in Visual Informatics. IVIC 2017. Lecture Notes in Computer Science*, Bangi, Malaysia, 2017. Doi: 10.1007/978-3-319-70010-6\_65.
3. Bekkouch S, Faraoun K. Robust and Reversible Image Watermarking Scheme Using Combined DCT-DWT-SVD Transforms. *Journal of Information Processing Systems*. 2015; 11(3):406-420. Doi: 10.3745/JIPS.02.0021
  4. Benoraira A, Benmahammed K, Boucenna N. Blind image Watermarking Technique based on Differential Embedding in DWT and DCT Domains. *EURASIP Journal on Advances in Signal Processing*, 2015, 1-11. Doi: 10.1186/s13634-015-0239-5
  5. Chen S, Huang H, Kung W, Hsu C. Optimization-based Image Watermarking with Integrated Quantization Embedding in the Wavelet Domain. *Multimedia Tools and Applications*. 2016; 75(10):5493-5511. Doi: 10.1007/s11042-015-2522-8.
  6. Coolidge FL. *Statistics: A gentle Introduction*. SAGE Publications, 2012. ISBN: 9781412991711.
  7. Das S, Kundu MK. Effective Management of medical Information through Roi Lossless Fragile Image Watermarking Technique. *Computer Methods and Programs in Biomedicine*. 2013; 111(3):662-675. Doi: 10.1016/j.cmpb.2013.05.02.





**Chapter - 3**  
**Solar Photo-Fenton Degradation of Trypan Blue  
Dye in Wastewater: Batch Kinetic Study**

**Authors**

**P. Shanthi Priya**

Assistant Professor, Department of Mechanical, Malla Reddy  
Engineering College (A), Secunderabad, Telangana, India

**P. Neha**

Assistant Professor, Department of Mechanical, Malla Reddy  
Engineering College (A), Secunderabad, Telangana, India



# Chapter - 3

## Solar Photo-Fenton Degradation of Trypan Blue Dye in Wastewater: Batch Kinetic Study

P. Shanthi Priya and P. Neha

### Abstract

Azo dyes are discharged in large quantities from the dye and textile industries as well as from the pulp and paper industry. Zollinger (1987), Robinson *et al.* (2001) and Ogugbue *et al.* (2011) reported that over  $7 \times 10^5$  ton of dye-stuff is produced and consumed annually all over the world. Due to their chemical structure, dyes are resistant to fading on exposure to light, water and many chemicals (Poots and McKay, 1976; McKay, 1979). Many dyes are difficult to decolourise due to their complex structure and synthetic origin reported that 10-15% dyes are released into the environment during dyeing process generating highly colored effluents. Colour in wastewater makes it aesthetically displeasing and the darkness of colour inhibits penetration of light deeper into the water interfering with the life-processes of aquatic plants and animals. These colouring materials are often toxic and hazardous, carcinogenic or mutagenic to life forms because dyes can remain in the environment for a long period of time and therefore, adequate treatment procedure becomes necessary. Biodegradation is generally a well-accepted and economical technique for industrial wastewater. However, some of the organic pollutants like dye and pesticides are not biodegradable. Sometimes they are carcinogenic and mutagenic. Azo-dyes and organophosphate pesticides are such type of organic pollutants. As described in the literature, there are different processes available for wastewater treatment.

**Keywords:** solar, CPC, SCR

### 1. Introduction

Dye is being extensively used as colorants in textile industries. Treatment of colored wastewater is one of the major problems faced by the industries involved in dyeing process. According to many researchers (Bukallah *et al.*, 2007; Trovo *et al.*, 2013), azo dyes damage ecosystems

when discharged into natural water and cause serious health risks to humans. Treatment of azo dye-containing water is difficult because of their high biological and chemical oxygen demands and high toxicity. Different AOPs were reported to be applied in oxidization of organic pollutants. Among the AOPs, solar photo-Fenton process has been successfully used to treat a wide variety of contaminants at laboratory scale. The present chapter reports the degradation of an azo dye pollutant (Trypan Blue) by solar photo-Fenton oxidation in a box-type photo reactor under batch mode. The effective process parameters were identified to be

- i)  $\text{H}_2\text{O}_2$  and  $\text{FeSO}_4$  dosing.
- ii) pH.
- iii) Initial concentrations of the substrate.

Extent of mineralization in the treated wastewater was studied by the decrease in the respective Chemical Oxygen Demand (COD). Generally, photo-Fenton reactions are reported to be carried out at  $\text{pH} \leq 3.5$  (Zheng *et al.*, 2007; Fernandes *et al.*, 2014); however, it imparts an additional acid loading, which needs neutralization before discharge. Moreover, the cost would increase due to the acid-resistant equipment and the process of acidification and neutralization. Therefore, in the present investigation, the reactions were carried out at near neutral pH. When natural water is exposed to sunlight, it is evident that there are some photo-Fenton reactions at circum-neutral pH. Additionally, the well-known statistical technique of Response Surface Methodology (RSM) was applied to optimize the aforementioned process parameters. A kinetic rate model, specifically suitable to predict the start up rate was proposed and validated with respect to the experimental data.

## **2. Objectives of work**

Based on the above scope of work, the objectives of the work are detailed as below: To Study the photo-Fenton oxidative degradation of Trypan Blue dye and Dichlorvos pesticide with sunlight and UV light in batch processes. Additionally, to design and optimize the process parameters by Response Surface Methodology (RSM). Comparative performance analysis of the two sources of light (sunlight and UV) and comparison between different intensity of UV radiation with study of the effects of seasonal variation of sunlight on the degradation of different organic pollutants. To design and develop a continuous solar reactor from the batch process data for photo-Fenton treatment of dye and pesticide in water. Testing the performance of the developed reactor and optimization of

process parameters. Development of mechanistic models and rate equations, followed by the validation of the same with respect to the experimental data obtained from batch and continuous processes. Testing of the net toxicity of treated water using a suitable biomarker, for example. *Nostoc* sp. Testing the efficacy of the processes and the reactors with real life wastewater collected from dyeing industry.

In most studies, photo-Fenton experiments are conducted using UV radiation. Reports on the use of sunlight are comparatively fewer. Even if some studies have been done in sunlight, many of them have used solar simulators. Use of direct sunlight with seasonal variation, in the photo-Fenton degradation of organic pollutants is a relatively unexplored domain. Fenton reaction is generally effective in acidic pH (about 3); however, the treated wastewater cannot be directly discharged to the natural water bodies because of this high acidity. Neutralization by alkali increases total dissolved solid as well as the operating cost of the process. To address this problem solar photo-Fenton oxidation of the dye-pollutant (Trypan Blue) has been planned to be carried out in near-neutral pH. 61 This is a rare and novel study and modelling of rate equation at neutral pH is also scarce if not unavailable till date. Continuous reactors available for solar Fenton reaction are generally fitted with concentric parabolic collectors (CPC). These are difficult to fabricate and maintain. In this work, a non-concentrating type, open-channel, continuous solar-collector reactor (SCR) has been developed. This is rather unconventional and its efficacy has been planned to be examined both by simulated wastewater and real industrial effluent. The simulated wastewater separately contained Trypan Blue dye and Dichlorvos pesticide, whereas actual wastewater obtained from a jute-dyeing industry contained dye pollutant. As per our knowledge, this type of reactor has not been used for solar photo-Fenton reaction before, which clearly signifies the novelty of the present research. Homogeneous Fenton reaction ( $\text{Fe}^{2+}/\text{H}_2\text{O}_2$ ) is one of the most important advanced oxidation processes to generate (Formula presented.) free radicals for degradation of organic pollutants in wastewater. Degradation of an azo dye (Trypan Blue) by solar photo-Fenton process has been investigated in this work using a batch reactor under sunlight. Instead of acidic pH used in conventional Fenton reaction, neutral pH is used here to modify the same. Effects of the changes in process parameters, including dosage of ferrous sulphate and hydrogen peroxide as well as pH have been examined. Percent degradation was observed to increase with increasing  $\text{H}_2\text{O}_2$  dosing up to a particular critical value. Increase in  $\text{FeSO}_4$  dose and acidic medium increased degradation.

## Scope of work

Scope of the present research work is given below Examination of the efficacies of UV and sunlight assisted photo-Fenton degradation of organic pollutants such as dye and pesticides in batch processes with varying process parameters. Designing and characterization of a continuous reactor from the batch kinetic data and checking its efficacies for degradation of the same organic pollutants. Study of the mineralization and ecotoxicological impacts of the treated wastewater. Optimization of the process parameters as well as kinetic modelling for the batch and continuous processes. The scope is schematically represented as follows for better understanding:

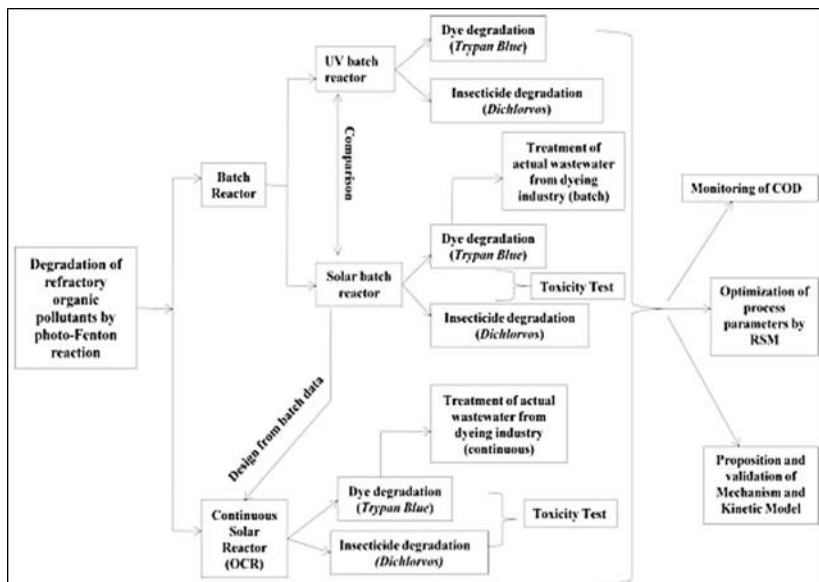


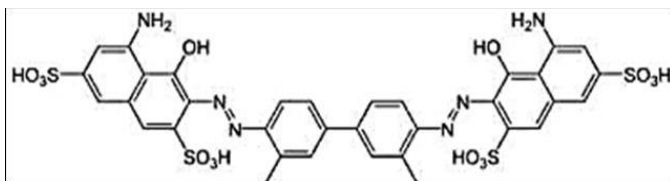
Fig 1: Schematic of the scope of work

## 3. Experimental analysis

### 3.1 Chemicals

Trypan Blue dye (Chemical formula  $C_{34}H_{23}N_6Na_4O_{14}S_4$ , molecular weight 960.80 and C.I. No. 23850) manufactured by Loba Chemie, Mumbai, India was procured. Chemical structure of Trypan Blue is illustrated in Fig. Hydrogen peroxide ( $H_2O_2$ , 50% v/v) was purchased from Merck Specialities Private Limited, India. Crystalline ferrous sulfate ( $FeSO_4 \cdot 7H_2O$ ) was procured from Sisco Research Laboratories Private Limited, India. Different volumes of 0.5%  $FeSO_4$  solution and 50%  $H_2O_2$  solution were used for reaction. pH of the dye solution was adjusted with 0.1(N) solutions of

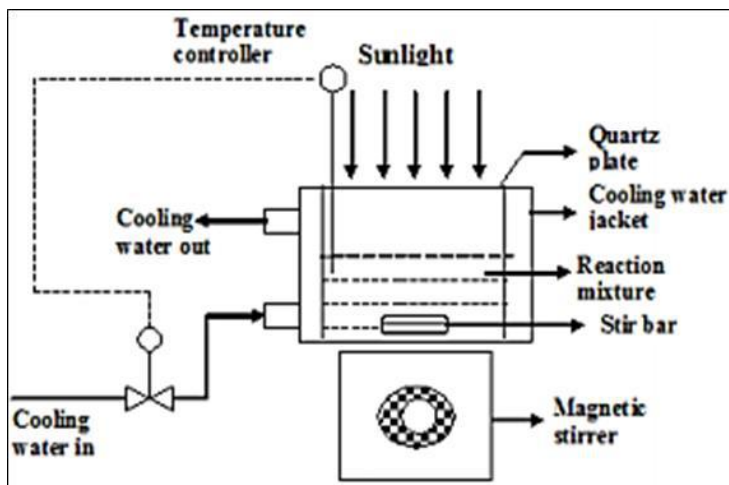
sulphuric acid (H<sub>2</sub>SO<sub>4</sub>) or sodium hydroxide (NaOH). Sodium bi-sulphite (NaHSO<sub>3</sub>) was procured from Loba Chemie. 5.00 (N) NaHSO<sub>3</sub> solution has been used to stop the Fenton reaction at the desired point.



**Fig 3.1:** Chemical structure of Trypan Blue dye

### 3.2 Experimental procedure

All the experiments were carried out under batch mode within the time span between 12 noon to 2 pm, during April-May months in 2012 in eastern part of India (22.5785° N, 88.3727° E). The photo reactor is a stainless-steel box (23.2cm × 23.2cm × 8.1cm), provided with a cooling water jacket and a quartz sheet (14.2cm × 14.2cm) as the top-cover for easy accessibility of sunlight. The reactor is fitted with a magnetic stirrer to ensure concentration homogeneity. Fig. 4.2 shows the schematic of the experimental set-up. Initially, 500 mL of dye solution of specific concentration was taken in the reactor. Prefixed volumes of FeSO<sub>4</sub> and H<sub>2</sub>O<sub>2</sub> solutions were added and the reaction mixture was vigorously stirred. Aliquots of samples were withdrawn at different time intervals to determine the extent of reaction and mineralization. The residual dye was analyzed using spectrophotometer. The reaction was terminated using 3.0 μl of 5(N) NaHSO<sub>3</sub> solution.



**Fig 3.2:** Schematic of experimental set-up

### 3.3 Analytical methods

Residual dye present in the solution was monitored by Shimadzu 160A UV-vis spectrophotometer at  $\lambda_{\text{max}} = 590$  nm using 1 cm optical path against a standard calibration curve, generated a priori. Chemical Oxygen Demand (COD) was determined by standard open reflux method, as described in APHA handbook (Rice *et al.*, 2005). pH was measured with properly calibrated pHtestr 20 instrument. Intensity of solar radiation was measured with Metravi 1332 digital lux meter. The intensity has also been reported in W.m<sup>-2</sup> using the conversion factor by Thimijan and Heins (1983). FTIR analysis was performed in a Jasco6300 instrument using KBr pellet.

### 3.4 Experimental design by response surface methodology (RSM)

Experiments were designed and process parameters were optimized by applying Response Surface Methodology (RSM, Design Expert version 7.0). The dosing of H<sub>2</sub>O<sub>2</sub>, FeSO<sub>4</sub> and pH were chosen as the control factors to be optimized. The process optimization was carried out with respect to the experimental data obtained at 120 min, just before terminating the Fenton reaction. These ranges and levels of each process parameter are presented in Table 4.1. For optimization of the process parameters, using central composite design scheme it has resulted into twenty experimental runs, with % degradation as the sole response. The parametric locations of all the experimental runs are presented in Table 4.2, which represents the complete set of the experimental design. The first step of the RSM was to find out a suitable functional relationship between the response and the set of independent parameters, which was followed by the subsequent optimization.

## 4. Results and discussion

### 4.1 Influencing process parameters

Influence of initial concentration of hydrogen peroxide H<sub>2</sub>O<sub>2</sub> has been found to play an important role in the decolourization of dye by photo-Fenton oxidation. No degradation has been found without hydrogen peroxide as observed in the blank experiment, conducted at the beginning of the experiment, keeping all the other experimental parameters at some arbitrary non-zero constant values. Initial dosing of H<sub>2</sub>O<sub>2</sub> was varied within the range of 0 to 0.058 mol. L<sup>-1</sup> and other experimental conditions, such as 65 initial concentration of dye ( $5.2 \times 10^{-4}$  mol. L<sup>-1</sup>), dosing of FeSO<sub>4</sub> ( $2.8 \times 10^{-4}$  mol. L<sup>-1</sup>) and pH (7.00) were kept unchanged. Time-concentration profiles for the degradation of dye with various H<sub>2</sub>O<sub>2</sub>-dosing are presented in Fig. 4.3 (a). For the initial H<sub>2</sub>O<sub>2</sub> dosing of 0, 0.014, 0.020, 0.024, 0.03, 0.044 and

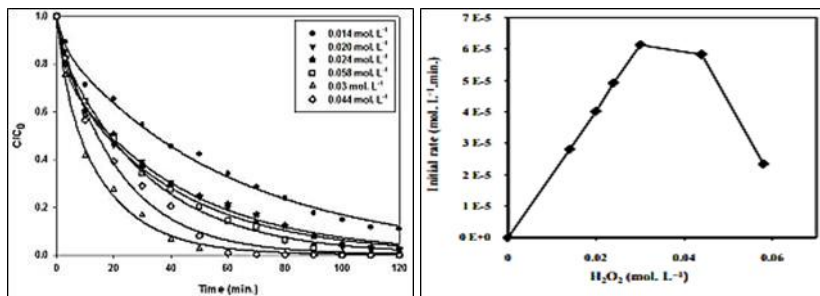


0.058 mol. L<sup>-1</sup>, the removal of colour after 120 min were 0, 89.16%, 97.39%, 97.84%, 100%, 99.26% and 97.90%, respectively. However, with the increase in H<sub>2</sub>O<sub>2</sub> dosing, the initial reaction rate of dye has been noted to increase up to a particular dosing of 0.03 mol. L<sup>-1</sup>. Further increase in the dosing of H<sub>2</sub>O<sub>2</sub> has resulted in the decrease of the initial rate of degradation as depicted in Fig. 4.3 (b). This may be attributed to the hydroxyl radical scavenging effect of H<sub>2</sub>O<sub>2</sub> at higher concentration of the later (Dutta *et al.*, 2002).

**Table 4.1:** RSM for the three experimental variables in coded units

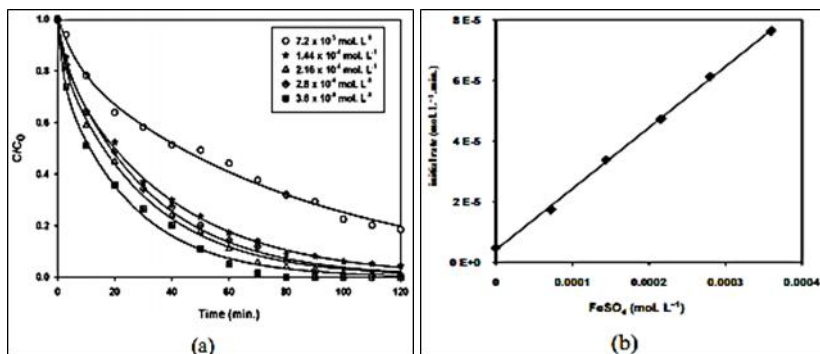
Run	Fe <sup>2+</sup> × 10 <sup>4</sup> mol.L <sup>-1</sup>	H <sub>2</sub> O <sub>2</sub> mol.L <sup>-1</sup>	pH	Experimental conversion (%)
1	2.80	0.030	3.0	100
2	2.80	0.030	4.0	100
3	2.80	0.030	5.0	96
4	2.80	0.030	6.0	94
5	2.80	0.030	7.0	93
6	2.80	0.030	8.0	80
7	0.00	0.030	7.0	08
8	7.20	0.030	7.0	80
9	1.44	0.030	7.0	94
10	2.16	0.030	7.0	98
11	2.80	0.030	7.0	99
12	3.60	0.030	7.0	99
13	2.80	0.014	7.0	88
14	2.80	0.020	7.0	96
15	2.80	0.030	7.0	99
16	2.80	0.044	7.0	99
17	2.80	0.058	7.0	88
18	0.00	0.00	7.0	00
19	2.80	0.030	3.2	98
20	2.80	0.030	4.8	91

Reduction of COD has increased with the increase in H<sub>2</sub>O<sub>2</sub> dosage up to a particular value and then decreased, as presented in Table 4.3. The maximum COD reduction has been found to be 53.2% at 0.044 mol. L<sup>-1</sup> of H<sub>2</sub>O<sub>2</sub> dosing.

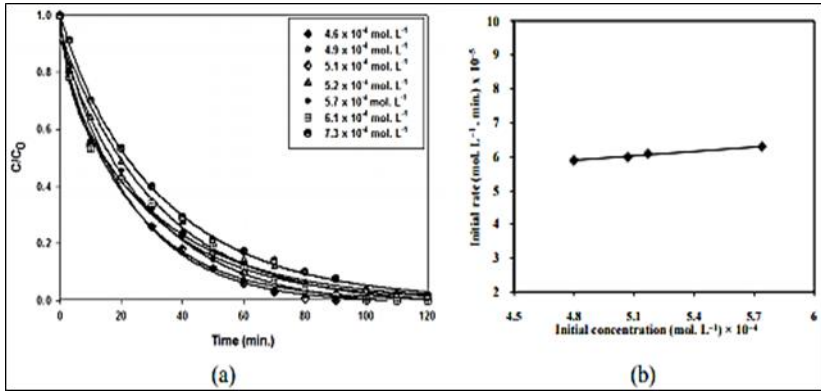


**Fig 4.1:** (a) Effect of H<sub>2</sub>O<sub>2</sub> on dye decolourization: time-concentration profiles, (b) Initial rate with increasing concentration of H<sub>2</sub>O<sub>2</sub>

Degradation of dye has been recorded to be 8% in an experiment conducted without adding ferrous sulphate and keeping all the other experimental parameters, such as initial concentrations of dye, dosing of H<sub>2</sub>O<sub>2</sub> and pH unchanged. This is because of non-zero H<sub>2</sub>O<sub>2</sub> dosing, which itself is an oxidising agent. Additionally, the initial dosing of FeSO<sub>4</sub>, was varied within the range of 0 to 3.6 × 10<sup>-4</sup> mol. L<sup>-1</sup> without changing H<sub>2</sub>O<sub>2</sub> dosing. It may be noted that FeSO<sub>4</sub> acts as the catalyst that enhances generation of OH• radical from H<sub>2</sub>O<sub>2</sub>. 39.94% of the initial dye has been observed to decolorize using only H<sub>2</sub>O<sub>2</sub> without adding FeSO<sub>4</sub>. The observation indicates that H<sub>2</sub>O<sub>2</sub> being an oxidizing agent can remove the colour partially; nevertheless, the presence of FeSO<sub>4</sub> catalyzes the oxidation reaction and therefore, enhances the rate of oxidative degradation. Requirement of FeSO<sub>4</sub> is small in the presence of sunlight. However, only FeSO<sub>4</sub> without H<sub>2</sub>O<sub>2</sub> could not degrade the azo dye.



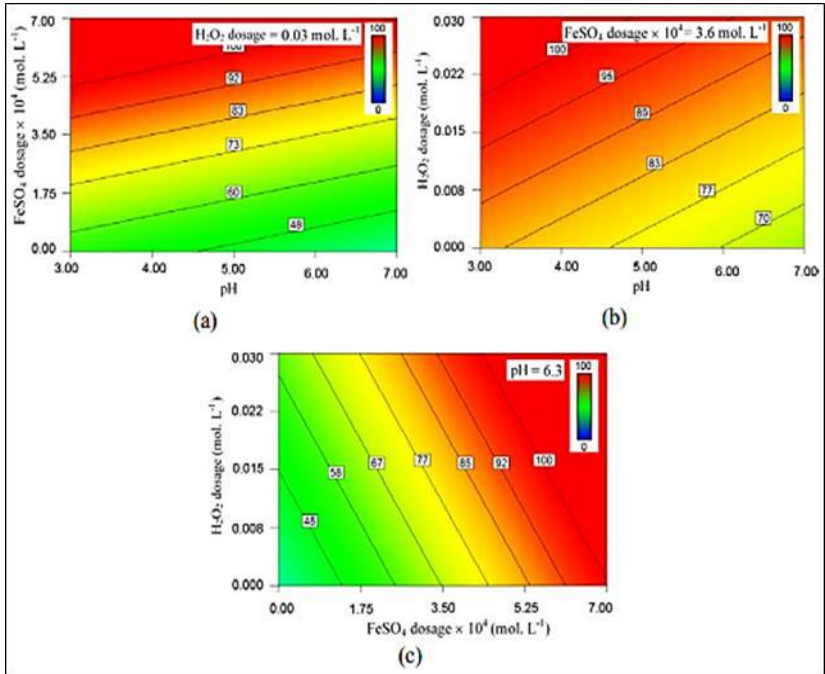
**Fig 4.2:** (a) Effect of FeSO<sub>4</sub> dosing on decolourization of dye: time-concentration profiles, (b) Initial rates at different FeSO<sub>4</sub> dosage



**Fig 4.3:** (a) Effect of initial concentration of dye: time-concentration profiles, (b) Initial rate vs. initial concentration.

**4.2 Determining the optimum process conditions**

After fitting the regression model, it has been observed that the present system can be best described by the linear regression model. Detailed ANOVA analysis for linear model was carried out to evaluate the effect of each parameter and their respective interactions. Model’s F-value of 375.49 implies the model is significant. There is only 0.01% chance that model Fvalue this large could occur due to noise. Values of “Prob > F” less than 0.05 indicate that the model terms are significant. It is well known that R2 always increases as we add terms to the model, whereas adjusted R2 statistic often decreases upon adding unnecessary terms. For the present model, proximity of R2 (= 0.986) and adjusted R2 (= 0.983) confirms the presence of significant terms only. Three different contour plots according to the final response surface are shown in the Fig.



**Fig 4.4:** Contour plot of response surface curve for decolonization showing interaction between (a) H<sub>2</sub>O<sub>2</sub> dosage, (b) pH and (c) FeSO<sub>4</sub> dosage

## Conclusion

Solar energy assisted photo-Fenton oxidation has been found to be pretty effective for the removal of Trypan Blue dye from wastewater in a set of batch experiments. Complete decolorization has been observed within 120 min, even though the experiments have been conducted at pH 7.0. This would save the cost of post-treatment neutralization of the treated wastewater and the total dissolved solid (TDS) load of the same. A kinetic rate model has been proposed and validated with the experimental data. The initial rate has been noted to increase with increase in the H<sub>2</sub>O<sub>2</sub>-dosing, up to an optimum value and remained independent of the initial concentration of the substrate within experimental range. Increase in the dosing of FeSO<sub>4</sub> has increased the initial rate. Optimum process conditions, as obtained from RSM are: pH = 6.5, H<sub>2</sub>O<sub>2</sub> = 0.03 mol. L<sup>-1</sup>, FeSO<sub>4</sub> = 3.6 × 10<sup>-4</sup> mol. L<sup>-1</sup>. Optimum % degradation has been recorded to be 100. Degradation products and reaction intermediates have been identified with FTIR and GC-MS analysis.

## References

1. Acero J, Benitez F, Gonzalez M, Benitez R. Kinetics of fenuron decomposition by single-chemical oxidants and combined systems. *Industrial & Engineering Chemistry Research*. 2002; 41(17):4225-4232.
2. Bringmann G, Kuhn R. Comparison of the toxicity thresholds of water pollutants to bacteria, algae and protozoa in the cell multiplication inhibition test. *Water Research*. 1980; 14(3):231-241.
3. Chiron S, Fernandez-Alba A, Rodriguez A, Garcia-Calvo E. Pesticide chemical oxidation: state-of-the-art. *Water Research*. 2000; 34(2):366-377.
4. Dantas TLP, Jose HJ, Moreira RFP. Fenton and Photo-Fenton oxidation of tannery wastewater. *Acta Scientiarum Technology*. 2003; 25(1):91-95.
5. Thampi Nitrogen, Nisha Radius. 'A powered water rolling synchro and streamlined deposit as well as verve management', ont. depart. ext. depend on. *Electr. Commun. Engg. (ijarece)*, quint, (2), journals, 2016, 338-342.
6. Slabbert Constant, Malengret K. 'Grid connected/solar pump for the reason that homespun areas'. *Rsa Ont. Symp. in the week heavy thermionics, mortal strike*. *Isie*. 1998; 21(000):31-34.



## **Chapter - 4**

### **Analysis of Digital Image Based on CT Scans**

#### **Authors**

##### **B. Mala Konda Reddy**

Associate Professor, Department of ECE, Narayana Engineering College, Gudur, Andhra Pradesh, India

##### **Rajesh Reddy Duvvuru**

Assistant Professor, Department of EEE, Narayana Engineering College, Gudur, Andhra Pradesh, India

##### **Ch. Narendra Kumar**

Associate Professor, Department of EEE, Malla Reddy Engineering College (A), Hyderabad, Telangana, India





# Chapter - 4

## Analysis of Digital Image Based on CT Scans

B. Mala Konda Reddy, Rajesh Reddy Duvvuru and Ch. Narendra Kumar

### Abstract

The digital image processing techniques, including gray level transformation, image sharpening, image segmentation and edge detection, is applied to the study on the meso-structure image of shale. The results show that the digital image processing technique can extract useful information from the CT images and construct a model of meso-structure of shale. The model shows the spatial distribution of the different media in the rock. The process of the damage propagation can be seen IN the meso-structure image clearly. Asphalt concrete is a composite material which consists of asphalt cement, voids, fine particles, sand, and coarse aggregates. Previous investigations of asphalt concrete mixtures have mainly concentrated on the macroscopic properties of the composite materials based on the assumption that the mixtures are homogeneous and isotropic.

**Keywords:** CT, MS, AC

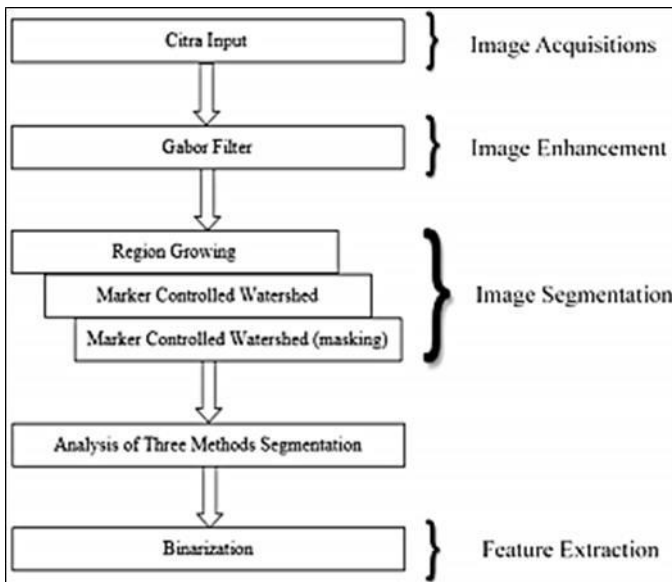
### 1. Introduction

Asphalt concrete (AC) is a composite material which consists of asphalt cement, voids, fine particles, sand, and coarse aggregates. These individual materials and components have different physical and mechanical properties and behaviour which have a significant effect on the performance of AC mixtures. It is well recognized that AC performance is also influenced by compaction methods and the quality and effort of compaction with the improvement and development of computer technology, the digital image processing technique has been developed to be an independent discipline, and it was applied widely in different disciplinary fields. However, the advantages of the technique have not been used fully in geotechnical engineering field. The treatment of CT images and their available information by using the digital image processing technique is seldom reported. In this paper, a digital image processing technique based on VC++ program is applied to acquire available information from CT images to make a study on the meso-structure characteristics of the rock.

## 2. Image processing technique

A CT image is essentially gray image, which consists of CT values. CT values can reflect internal density changes of a rock. The distribution of different materials in a rock's interior can be reconstructed by the changes of grey degree. The images can reflect the meso-structure of the rock well. The sample of CT scanning test comes from shale rock in Huangling in Shaanxi Province. The shape of the samples is a cylinder (50 mm10 mm), and the dry density is 2.43 g/cm<sup>3</sup>.

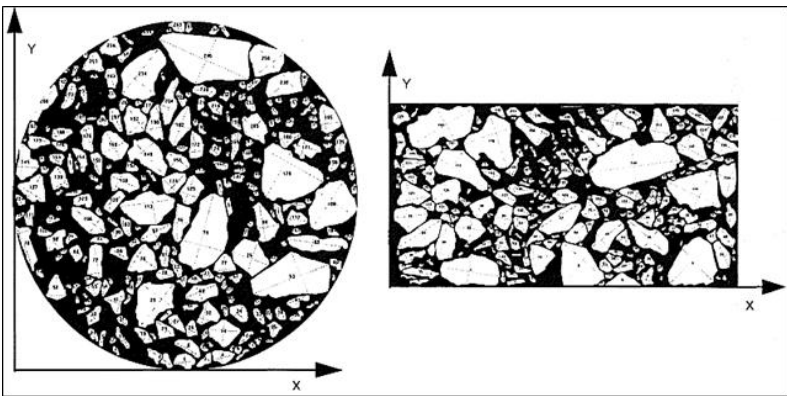
In Fig. 1, the three CT images are the images of the lower layer of a sample. They are in the condition of three deviatoric stresses (0MPa, 15MPa, 30MPa) respectively. The initial damage situation of the rocks, such as pores, grain boundary and meso-crack, can be seen in such CT images. Disorder distribution of the damages leads to uneven initial structure of the rocks. With the increasing damage deviatoric stresses, the scanning level has undergone a process of initiation, crack initiation, bifurcation, and damage destruction. Field cores or laboratory prepared AC specimens are cut using a circular masonry saw in multiple vertical or horizontal plane cross sections (Fig. 1). The AC cross sections are photographed with a ruler placed beneath the section for scaling and calibration in the digital image processing.



**Fig 1:** Image Processing for Lung cancer detection stages

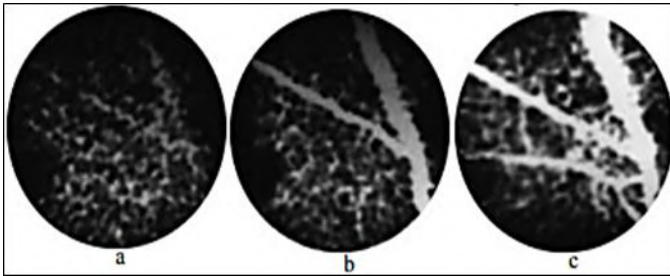
A Microtek flatbed scanner is used to convert the photographs into digital files that can be processed by a computer. The image is stored in a file

with. TIF format as series of pixels (or points). For a black and white print and a colour picture (4 in. by 6 in. (1 in. = 2.54 cm)), 300 dots per inch and 165 dots per inch were used, respectively. Each pixel has three digital values indicating the X and Y coordinates and grey level or colour intensity. It is noted that other systems are available for a direct input of a video image into a computer using a charge coupled device (CCD) camera (Eriksen 1993). However, such a system is quite expensive. An image editing software, called Picture Publisher (v.4.0), was then used to manually outline the boundaries of aggregates on the digitalized image. A manual technique was used because the image analysis software cannot satisfactorily and automatically recognize if a pixel is part of an aggregate or the asphalt matrix. The automatic recognition of aggregates produced poor results owing to the following facts.



**Fig 2:** Selected results for the basic measurements of aggregate cross sections

The study on the meso-structure images of shale cannot be carried out on a deeper level. By using the digital image processing technique, mesostructure of the rock material can be constructed. The whole process of constructing an image of the meso-structure of the rock can be seen in Fig. Gray level transformation is a kind of contrast stretching technique, which can not change the position relation of pixels of the original images. The feature can be helpful to do recognition and analysis for images. Gray equilibrium and gray stretch are two different, commonly used methods of gray level transformation. Gray equilibrium can improve the contrast of the whole image. Compared with the gray equilibrium, gray stretch only improves the contrast of the local gray range by linear transformation of gray in a segment.



**Fig 3:** CT image of shale rock in lower level in different damage propagation stage

Defects, such as cracks and pores, can be judged from CT images. However, quantitative evaluation of different sizes, shapes, and space positions cannot be done for defects. When the CT images are acquired and transmitted; some unnecessary noise has occurred to the CT images. An image smoothing technique has some different ways to operate on images. The median filter method not only can protect the edge of the images, but also can eliminate noise at the same time. Meanwhile, the images cannot become fuzzy.

The median filter method is applied to eliminate noise in the paper. Image sharpening is a good way for image enhancement. The method can make the fuzzy edges and the contour lines clearer. The details and edges of the images can be more prominent. For images, both differential operation and gradient operation can perfect the images. In the paper, Roberts gradient sharpening method is used to do the work. After the gradient operation for the CT images, the points, in which gray values have rapid changes, have been preserved in the end. Fig. 4 shows that the edge of the cracks in the CT. Modules and example of marker-controlled watershed segmentation method is existing in MATLAB software that can be directly used. Figure 3 shows the result of segmentation by using Marker Controlled Watershed.

### 3. Results

The process to get the segmentation by region growing method is as the following; firstly, select the area that will be the target object, which is the right lung and the left lung, then, put the seed in this area. Furthermore enlarge the size of the seed so that it covers all the desired areas. Figure 4 shows the result of segmentation by region growing method. To get the segmentation result of watershed method, the steps are as follows; firstly, calculate the distance gradient for edge detection, and then mark the target object by using a morphological technique called opening by reconstruction and closing by reconstruction. After marking object is revealed, other areas can be discarded.

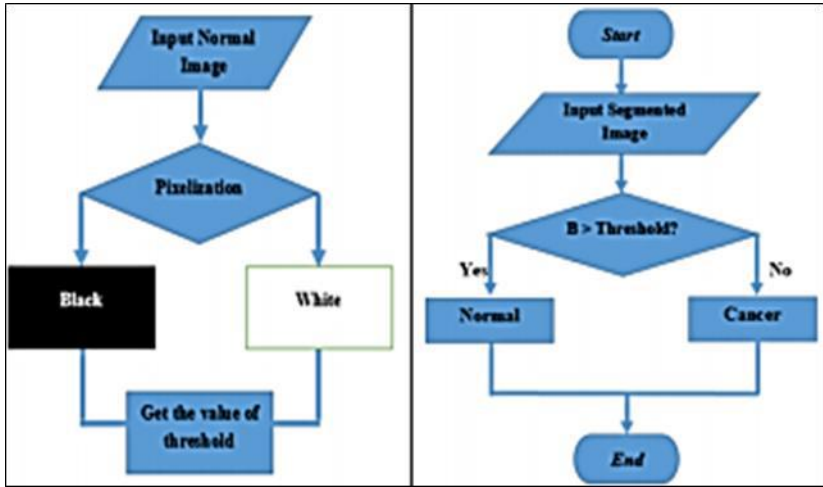


Fig 4: Pixelization and binarization scheme

The actual sizes of the samples would be transformed to image sizes. When a side length of a sample is divided by a side length in an image, a coefficient can be acquired, and it can be named conversion proportion. Conversely, the parameters of a polygon (ordinate and abscissa) after geometrical vectorization of the meso-structure image can be transformed to the actual sizes of the samples when it is multiplied by the coefficient. In the numerical calculation of ANSYS software, the material type can be determined at first, and thus the heterogeneity of the rock can be considered during the process of numerical simulation. By doing this, the FEM mesh model can be generated directly, which can be seen in Fig 5.

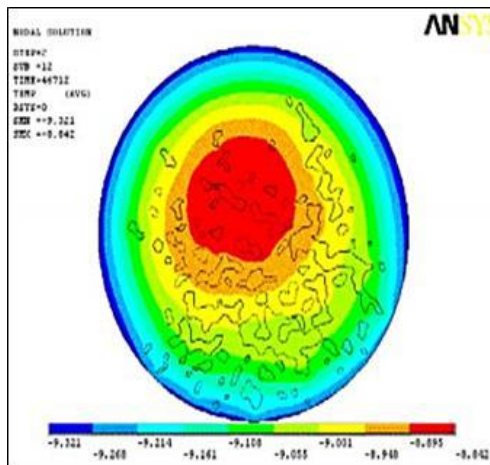
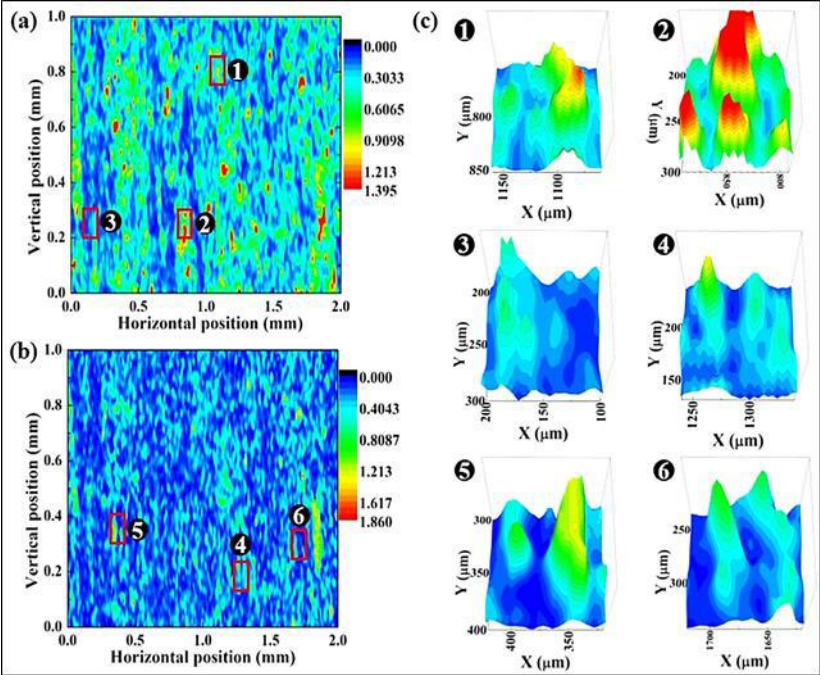


Fig 5: The transient temperature field of shale

The actual sizes of the samples would be transformed to image sizes. When a side length of a sample is divided by a side length in an image, a coefficient can be acquired and it can be named conversion proportion. Conversely, the parameters of a polygon (ordinate and abscissa) after geometrical vectorization of the meso-structure image can be transformed to the actual sizes of the samples when it is multiplied by the coefficient.



**Fig 6:** Different shapes of CT images

The underlying premise for breast cancer screening is that it allows for the detection of breast cancers before they become palpable. Breast cancer is a progressive disease and small tumors are more likely to be detected in early stage of disease, have a better prognosis and are more successfully treated [3]. mammography is the gold standard for imaging of the breast and detection of early breast cancer. However, this sensitive screening and diagnosis technique has high false-positive (Fp) rate. Some of the limitations are: inability to change image contrast or brightness, problem in detection of subtle soft tissue lesions (dense glandular tissues) and difficult to archive. Ultrasound uses some harmless and painless sound waves to produce a visual picture of the breast. Ultrasound is non-invasive, portable and versatile, it does not use ionizing radiations and it is relatively low-cost.

Ultrasound image analysis in general is complex due to data composition, which is described in terms of speckle information. Upon visual inspection, speckle consists of a relatively high grey level intensity, qualitatively ranging between hyper-echoic (Bright) and hypo-echoic (Dark) domain [4]. In the analysis of medical images, the advices from medical doctors are required to inspect the suspected regions, for benign lesions and/or malignant legions.

## **Conclusion and future scope**

### **Conclusion**

The digital image processing technique can extract useful information from the CT images, and thus construct a model of meso-structure of rock. The model can show the spatial distribution of the different media in the rock clearly. By a process, such as geometrical vectorization, scaling transformation and the realization of the FEM software interface, finite element grid model can be established finally. It can be a research foundation for the further study on the mechanical properties of rock. computed Tomography (CT) is a non-invasive technique to provide CT images of every part of the human body without superimposition of adjacent structures. Image processing with Adobe Photoshop, Image J, Corel PHOTO-PAINT and Origin software has been used in order to achieve good quality images for quantitative analysis.

### **Future scope**

There are various types of imaging modalities available for diagnostic purpose like X-ray, CT, MRI, mammography and ultrasound. Being a very simple, economical, easy availability, the ultrasound imaging modality became more popular and as a common imaging modality, hence the work has been undertaken. Through ultrasound image various factors are extracted from an image. As well as it detects organ and abnormalities present in the organ. There are many advantages of ultrasound imaging it became very popular.

### **References**

1. Sonij Grgic, Mislav Grgic, Marta Mrak. Reliability of Objective Picture Quality Measures, JEE. 2004; 55:1-2.
2. Eskicioglu AM. Image Quality and Their Measures and Their Performances, IEEE, 1995, 43.
3. Chang RF, Wu WJ, Moon WK, Chen DR. Automatic Ultrasound segmentation and morphology-based diagnosis of solid breast tumors. Breast Cancer Research and Treatment, 1989, 179-185.

4. Yu YJ, Acton ST. Speckle Reducing Anisotropic Diffusion, IEEE Trans. On Image Processing, 2002, 11(11).
5. Koo JI, Park SB. Speckle reduction with edge preservation in medical ultrasonic images using a homogeneous region growing mean filter (HRGMF), Ultrasonic imaging. 1991; 13:211-237.
6. Hill PR, Canagarajah CN, Bull DR. Image Segmentation using a Texture Gradient Bas Watershed Transform. IEEE Transactions on Image Processing, 2003.



**Chapter - 5**  
**Performance of Modal Analysis and Finite**  
**Element Analysis**

**Authors**

**S.C. Sireesha**

Assistant Professor, Department Mechanical, Malla Reddy  
Engineering College (A), Secunderabad, Telangana, India

**D. Lakshmi Sravanthi**

Assistant Professor, Department Mechanical, Malla Reddy  
Engineering College (A), Secunderabad, Telangana, India



# Chapter - 5

## Performance of Modal Analysis and Finite Element Analysis

S.C. Sireesha and D. Lakshmi Sravanthi

### Abstract

Modal analysis has become a major technique to solve vibration problem. Finite element method (FEM) and experimental modal analysis (EMA) is a method to measure and analyze the dynamic response of complex structures. These two methods have important role to extract the modal parameters such as such as natural frequency, damping ratio and mode shape. Finite element analysis is engineering software that uses finite element method to analyze and determine the structure design in order to meet the performance criteria. Since the finite element method is computer aided software, so it needs to be design in CAD software such as Abacus, Autodesk Simulation, ANSYS, and CATIA. Experimental modal analysis has grown progressively since the advent of the digital FFT spectrum analyzer. There is several method used in EMA such as impact and shaker test but the frequently used is impact hammer test Finite element analysis (FEA) is a well known numerical technique for determining the dynamic characteristics of any mechanical structure. However, the results obtained by FEA are often error prone due to modelling errors or incorrect boundary conditions. In the present work, the experimental modal analysis of a rectangular plate with known geometric holes is conducted to determine the vibration characteristics

**Keywords:** FEA, ANSYS, CATIA

### 1. Introduction

Structures have made important advancements during the last some decades with the advancement of their aesthetic appeal, long span capability, quick and efficient construction, and their ability to make full and efficient use of material. Dynamic design aims at obtaining desired dynamic characteristics in machines and structures, which may include shifting of natural frequencies, mode shapes which are required and vibratory response.

The conventional dynamic design is basically hit and trial method in which we try to achieve desired dynamic characteristics by producing several prototypes. Computer modelling, usually finite element analysis (FEA) has been extensively used within the structural industry to aid in the design process of new product. FE modelling has been shown to be capable of predict the required mechanical properties of a structure that will give the desired performance characteristics. in this paper we have developed computer models to study the effect of natural frequencies and compare FE data with the experimental results to validate the model. FE modelling has been shown to be a useful tool in optimizing performance characteristics it is also a useful technique that can be used to reduce the time and financial cost of designing and manufacturing a new structure. Before a new design of a structure can be manufactured on the production line, the engineers must first be satisfied that the end product will have the desired mechanical properties. Before the advent of computer modeling, the traditional method was to manufacture prototypes, which were then subjected to mechanical tests to measure the structure's properties This process would have to be repeated until a prototype satisfied all the test requirements. An accurate FE model can be used to predict the mechanical properties of the manufactured structure without the need for numerous prototypes. To ensure that an FE model is accurate it needs to be validated. Modal analysis can be used as a method to dynamically validate the FE model by comparing its first few modes of vibration with experimental modal analysis data from the matching manufactured part.

## 2. Finite element modelling

The following section deals with the FE modelling of a rectangular plate. First a model of rectangular pate having one circular and a triangular hole. The plate 3-D model is created in ANSYS with web structure established in ANSYS. Material properties were defined as isotropic.

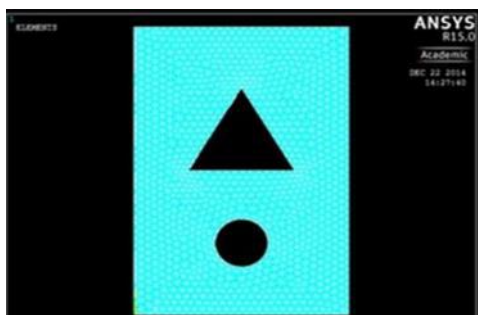


Fig 2: 1 FEM Plate model

The material properties were defined by the Material Models menu. The corresponding real constants were distributed to every part of the plate and appropriate grid size was set. All the areas were meshed by MASHTOOL in the way of Free The plate was modelled using solid 185 tetrahedral elements. The modal superposition method was used to compute the harmonic response of the FEM model. The difference between the experimental data and the FEM data is the result of shifting of the resonance frequencies. The largest shift (about 5 percent) occurs at the fourth resonance frequency. Thus, the FEM model is stiffer than the real system. There are four modes in the frequency range 100 to 500 Hz. All the mode shapes from the FEM model share the same trend and shape with their 100 200 300 400 500 counterparts from the experiment.

### 2.1 Dynamic finite element analysis of the plate

Dynamic finite element analysis of the plate mainly refers to the vibration modal analysis using the finite element theory. Modal analysis is used to identify natural frequencies, especially low-order frequencies and vibration modes of the plate. From the modal we can learn in which frequency range the plate will be more sensitive to vibrate. Plate should be designed to avoid the resonance region with the tower and other components in order to prevent some destruction of related components. In this paper, the finite model of the plate has been established in ANSYS by importing the plate model created previously.

### 2.2 Modal analysis of the plate

There are many ways for ANSYS modal analysis, of which the Block Lanczos method is most widely used because of its powerful features. Moreover, it is frequently applied with model of solid units or shell units.

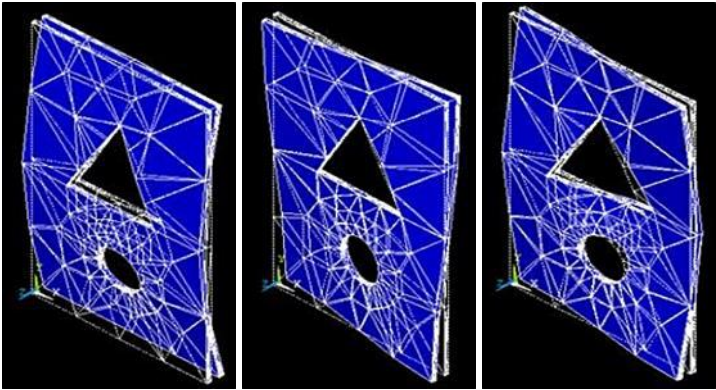


Fig 2.2: Different Shapes of plates

The vibration modes of the first six orders were extracted with the frequency range of 0~1500Hz. The connections of plate with the frame could be regarded as free, so all DOFs are free as modal analysis does not require applying loads. At last, after solving with the solver, the vibration modes of all the orders and the result of frequencies could be observed in the post-processor.

**Table 2.1:** FE results from ANSYS

Mode	I	II	III
Frequency (Hz)	210	230	375

### 3. Experimental analysis

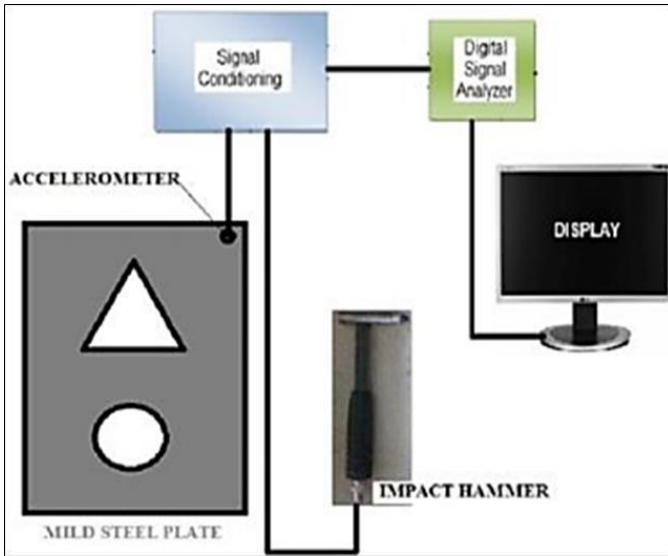
The specimen for analysis is prepared from the stock of commercial mild steel rectangular plate. The dimensions of the plates are randomly selected as preferably available in the stock. Further, in order to fabricate the plates, two irregularities are induced in plate one is circular and other is triangular, the dimensions of both holes are taken randomly. The photographs of the involved specimen to be analyzed are shown in the following fig 5.4 The dimension of rectangular plate is: (Length x width x thickness) = (300mm x 200mm x 5mm), Diameter of circular hole = 50mm, Dimension of equilateral triangle = 100mm each side, Weight of plate = 2100gms, Poisson ratio ( $\nu$ ) = 0.3 The experimental setup consists of a specimen that is in the form of a rectangular plate consisting of a circular and a triangular hole. The modal testing of this MS plate specimen has been done by supporting on the soft springs to achieve free-free conditions.

The various equipment involved in the apparatus required to perform the experiment are:

- 1) Accelerometer (Model 352C68 SN 66757) PCB Piezoelectronics, USA.
- 2) Signal conditioner (2Nos.) Model 480E09 (ICP Sensor Signal Conditioner) PCB Piezoelectronics, USA.
- 3) Digital Signal Analyzer (Signal Calc ACE).
- 4) Impact hammers PCB Piezoelectronics, USA.

The setup is arranged in order to perform the experiment has a rectangular MS plate with circular and triangular hole as mentioned above. The plate is marked with six points which represents as nodes named from 1 to 6. Further, an accelerometer is attached at the node 1 with help of wax. Now the impact hammer is made to strike the plate at the remaining nodes

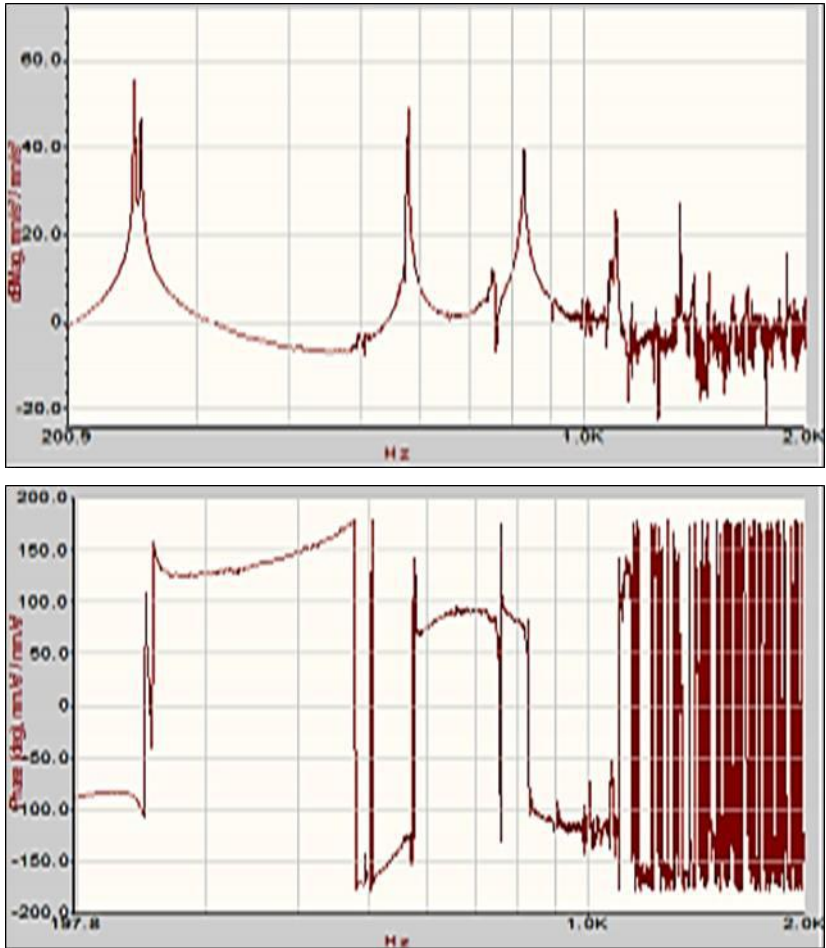
from 2 to 6 to measure the transfer mobility. Due to these excitations at various nodes vibrations are produced in the plate which are sensed by the accelerometer placed at node 1 and the effect at the respective node is transferred to the signal conditioner which conditions the signal or converts these signals into measurable form. The digital signals so obtained from the signal conditioner are provided to the digital signal analyzer which analyzes these signals and helps the software to plot the suitable FRF curve. The procedure is again repeated for various nodes one by one and their respective FRF curves are obtained.



**Fig 3.1:** Experimental setup of plate

#### **4. Comparisons of analytical and experimental results**

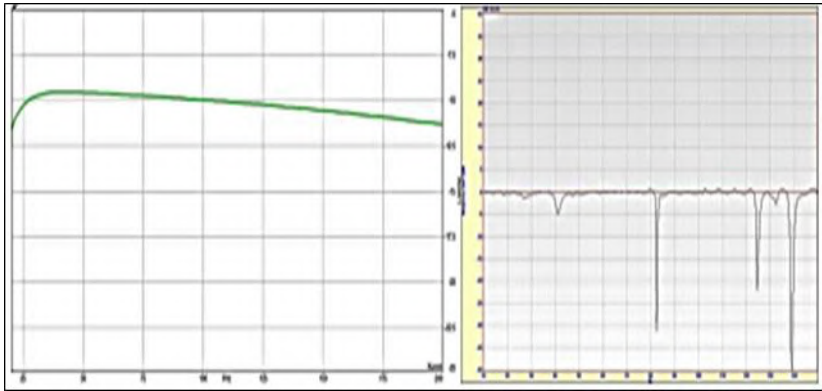
The first stage of any reconciliation exercise is to determine how closely the experimental and analytical models correspond. If we are unable to obtain a satisfactory degree of correlation between the initial analytical FE model and the test data, then it is extremely unlikely that any form of model updating will succeed. Thus, a successful correlation is crucial for the success of model updating. Table gives the comparison between experimental and analytical natural frequencies, for the first two modes, obtained from both the studies. If there are differences between analytical FE model predictions and experimental results, which is due to assumptions and approximations involved in the FE model the FE models need to be updated. However, the differences between the corresponding results of both studies are minor.



**Fig 4.1:** FRF of the plate

Apart from natural frequency comparison (as given in Table 2), another method of model correlation is mode shape comparison. To compare the mode shapes, we plot the deformed shapes of the structure for a particular mode, using experimental as well as analytical model. These mode shapes are plotted side-by-side for quick comparison. This is a graphical approach to model correlation.





**Fig 4.2:** Force spectrum and imaginary part of point FRF for Model

Experimental modal analysis was performed on the structure in free-free conditions using the FRFs. The FRFs were measured by impact excitation with an instrumented modal hammer while the responses were recorded by accelerometers. Excitation points were carefully selected to avoid missing any mode within the frequencies of interest. During tests, imaginary part of the point FRF and its force spectrum are checked to be confident for sufficient excitation as shown in Figure

**Table 4.1:** Comparison of experimental and FE natural frequencies

S. N.	Modes	FEM	EMA	% error
1.	I	210	232	-0.014
2.	II	230	245	-0.065
3.	III	375	380	-0.013
4.	IV	418	420	-0.004
5.	V	629	630	-0.001

FEA is the suitable tool for numerical modeling in structural engineering because it have ability of handling complex structural geometry, large complex assemblies of structural components and can build many different types of analysis [3]. BIW structure can be considered as a complex structure and modelling the structure to the actual might be difficult.

Thus, major simplification in modelling the structure was carried out with FE model.

FEA is the suitable tool for numerical modeling in structural engineering because it have ability of handling complex structural geometry, large complex assemblies of structural components and can build many different types of analysis [3]. BIW structure can be considered as a complex structure and modelling the structure to the actual might be difficult.

Thus, major simplification in modelling the structure was carried out with FE model.

FEA is the suitable tool for numerical modeling in structural engineering because it has the ability of handling complex structural geometry, large complex assemblies of structural components and can build many different types of analysis [3]. BIW structure can be considered as a complex structure and modelling the structure to the actual might be difficult.

Thus, major simplification in modelling the structure was carried out with FE model.

In this study, a suitable linear FE model of structures with rubber sealed glass is built. This modeling technique, adjusted by the measured modal properties of this structure, has been achieved by comparing natural frequencies and their mode shapes. However, these modal parameters may depend on types of sealing method and properties. This study also gives an opportunity to examine the effects of the sealing properties to select.

Experimental modal analysis was performed on the structure in free-free conditions using the FRFs. The FRFs were measured by impact excitation with an instrumented modal hammer while the responses were recorded by accelerometers. Excitation points were carefully selected to avoid missing any mode within the frequencies of interest. During tests, imaginary part of the point FRF and its force spectrum are checked to be confident for sufficient excitation as shown in Figure 4. If the energy distribution is proper while excitation, the imaginary part of point FRF is either entirely negative or positive in all interested frequencies. Being negative or positive is affected by the direction of the impact according to the response direction. Force spectrum is one of key properties for confident FRF measurement with impact hammer. For confident FRF measurement, the decrease of the level should not be more than 20dB in interested frequency band.

## **Conclusion and future scope**

### **Conclusion**

The finite element analysis of a rectangular MS plate has been carried out using ANSYS and an experimental test has been performed on the same using an experimental setup the results obtained from both the results have been compared and both the results shows a good agreement with each other. However, the post analysis on frequency response function (FRF) obtained from the experiment have not carried out (which is not required in this case due to close correlation). Thus, FE results have been verified using experimental results.

## **Future scope**

- 1) The identification of damping was applied to discrete models with two degrees of freedom only. It may be extended to more degrees of freedom and on real structures such as beams and frames. This study can be extended with real data obtained through experiment. This method can be extended to identify viscous and proportional damping in the structures.
- 2) The effect of noise and other forms of damping using experimental data can be done for identification of damping in future.
- 3) Dynamic design studies can be extended to more general cases and complex structures. The effect of damping and damped models can be included in dynamic design of mechanical structures.

## **References**

1. Baruch M, Bar-Itzhack IY. Optimal weighted orthogonalization of measured modes. *AIAA Journal*. 1978; 16(4):346-351.
2. Baruch M. Optimization procedure to correct stiffness and flexibility matrices using vibration tests. *AIAA Journal*. 1978; 16(11):1208-1210.
3. Berman A. Mass matrix correction using an incomplete set of measured modes. *AIAA Journal*. 1979; 17:1147-1148.
4. Berman A, Nagy EJ. Improvement of a large analytical model using test data. *AIAA Journal*. 1983; 21:1168-1173.
5. Bais RS, Gupta AK, Nakra BC, Kundra TK. Studies in dynamic design of drilling machine using updated finite element models. *Mechanical Mach Theory*. 2004; 39:1307-1320.



## **Chapter - 6**

### **Assessment of Real Time ID using RFID**

#### **Authors**

##### **P. Sree Lakshmi**

Associate Professor, Department of ECE, Audisankara Institute of Technology, Gudur, Andhra Pradesh, India

##### **Raja Reddy Duvvuru**

Associate Professor, Department of EEE, Malla Reddy Engineering College, Hyderabad, Telangana, India

##### **D. Saritha**

Assistant Professor, Department of CSE, Narayana Engineering College, Gudur, Andhra Pradesh, India



# Chapter - 6

## Assessment of Real Time ID using RFID

P. Sree Lakshmi, Raja Reddy Duvvuru and D. Saritha

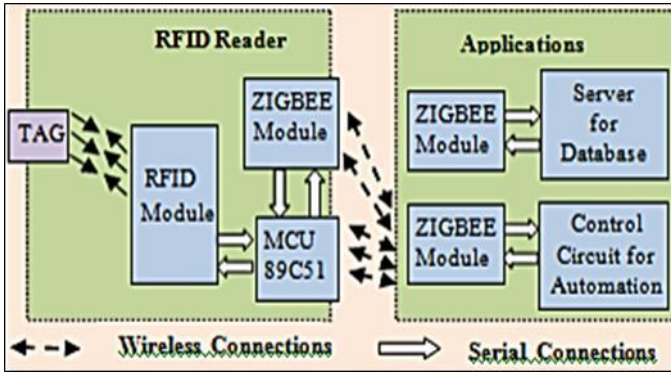
### Abstract

There is an inability to prove identity of a resident in many countries including India due to their population complexities which reflects the strongest hurdle on the way of imparting the government benefits to the deserving citizens of those countries. One has to go through a process of establishing his/her identity while seeking any concession to be drawn as per the applicability from their respective governments. However, finding a common platform to recognize the authenticity is a major challenge for both i.e. the government agencies and to its citizens [Ami 2016]. The area of National identity system has always received a huge degree of interest from various legends. Amongst them a one of the most notable ones former India, Ex-President and His Excellency APJ Abul Kalam who said about it that “It should be a multipurpose, secure and authentic ID card. This card should be akin to the Xerox copy of the individual with the multifactor authentication such as photograph, biometrics-fingerprint, iris-based system and digital signature”.

**Keywords:** RFID, E-ID, real time

### 1. Introduction

RFID is a very promising technology in terms to locate an object, real-time tracking. Its applications become wider when it comes to work along with IoT (Afzal *et al.*, 2020), where the combination of different devices is working and collecting the data from different sources. The technology for RFID tags is growing continuously. The not unusual notion is that the generation can be prepared for POC programs in 3-5 years. It is possibly that most institutions planning remedy administration protection tasks will first use barcodes in place of RFID tags. Since those safety initiatives involve a paradigm alternate in administration techniques, this has a tendency to go beyond any person's technology concerned in the process; thus, it's miles encouraged that establishments start their implementation without waiting for RFID era.



**Fig 1: Block Diagram for RFID System**

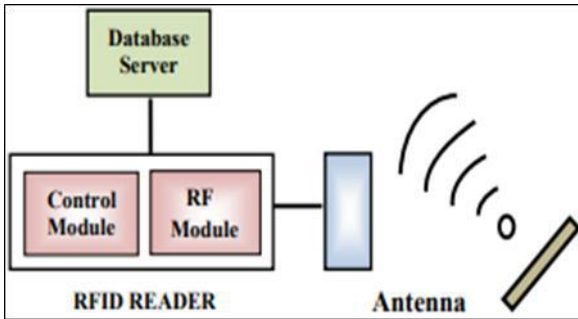
If RFID matures to the point of viability, it could be viable at some future date to alternative RFID tags for barcodes and RFID scanners for barcode scanners with little interruption to the system. Before adopting the RFID some issues should keep in mind before implementing this technology. Advancement in RFID tag makes it more compatible along with printed sensors, printed batteries, and thin-film photovoltaic. RFID is one of the main part of sensor systems which enables the organization to enhance the capability of better monitoring and assets management. It seems that adoption of RFID technology is slow but as far as health industry is concerned, the contribution of this technology is immense. The implementation of RFID system over barcode technology is minimal error of the system. Therefore RFID technology has an edge over barcode. In RFID tag if we compare barcode with RFID, in barcode human intervention is needed while RFID eliminates the human involvement in RFID system. The capability of reader is more than in barcode technologies as well as tag in RFID system has the ability to store large amount of data. So RFID system in healthcare is more reliable especially when it is compatible with IoT (Tayyaba *et al.*, 2020).

## 2. RFID Readers and network (TCP/IP) protocols

A RFID tag is activated when the antenna associated with the tag emits the radio signal to read/write the data on it. The distance covered by the radio signal depends on its radio frequency and the power output. A reader's activation signal is detected by the RFID tag whenever it passes to an electromagnetic zone [Liu 2017]. The RFID tag has an integrated circuit which posses the encoded data. The reader passes this data after decoding it to the computer for processing. A simplified block diagram to explain this processing of data is shown above in Figure 6.1. A RFID reader is comprised



of one Control module consisting of a microcontroller chip to process the data and a radio frequency module. It is connected to a computer having a data base with respect to a particular application. RFID reader is also connected to an antenna which emits the associated radio frequency in conjunction with RF module. The use of an appropriate TCP/IP data network protocols are essential. Hence, these are required to be incorporated during implementation of deployment of RFID readers.



**Fig 2:** A Simplified Block Diagram of a RFID Reader

## 2.1 Principals of RFID system

The basic principal that governs a RFID tag functions as follows: A current is induced in an antenna when a magnetic field is generated by its associated reader. The microprocessor chip is powered by this current. Along with the chip, a condenser too is charged by the current to extend uninterrupted power in a Passive tag. However, in an active tag, instead a condenser a battery is used to power the chip. A command is received by the RFID tag on activation from the reader which in turn replies the request by forwarding its serial number [Liu 2017, Mak 2018]. The reader requires extending continuous power to the RFID tag during its reading cycle. The major components involved in the RFID technology are explained in brief as under.

## 2.2 The RFID system

In order to have a complete RFID system, only a reader and just few tags would be insufficient. Information about serial number of a product alone does not help much to keep track of an object. The real strength of RFID system is to have additional information fetched from backend with product details and comprised of a database and an interface where the RFID tag is scanned and where computation is performed. 6.1.3(b) Use of Frequency Bands in RFID: There are mainly three types of frequency bands as Low Frequency (LF), High Frequency (HF) and Ultra High Frequency

(UHF) being utilized in RFID applications. Frequency ranges for these bands vary from 30 KHz to 5.8 GHz as 30-500 KHz for LF, 10-15 MHz for HF and 850-950 MHz, 2.4-2.5 GHz, 5.8 GHz for UHF applications. LF application tag is faster and cheaper and used in relatively smaller applications. Though, these low frequency tags do have advantage in being least affected to operate in fluids or metal. HF tags hold the characteristics to offer better ranges but are costlier [Dag2014]. UHF tags have the best ranges up to more than 30 meters with higher transmission rates but they are most expensive. They differ in frequency ranges in applications in different countries and unlike LF & HF applications require license from that country for its use.

### 2.3 Power requirements in RFID

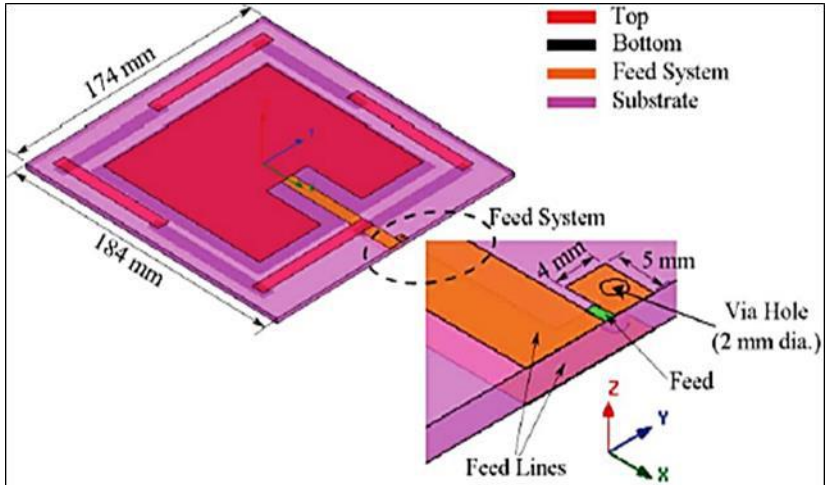
Power or energy requirements for passive, semi passive and active RFID tags vary. Passive tags are dependent on power provided by the reader and they do not have their own internal energy source. Therefore, without any need of a battery they are cheapest and smallest amongst all with longest lifespan but their ranges are limited to just few meters. The active RFID tags have an internal energy source to extend power to micro chip and for the antenna to produce a signal. These tags have best ranges amongst other types of RFID tags up to tens of meters with lifetime approximately up to five years.

6.1.4 Near and Far Field RFID Communication The fields initiate radiating in any magnetic field's region. The beginning of radiating fields is represented by the far field. However, once we move further, the strength of magnetic fields diverges with the cube inversely to the expanse from the equipment's antenna ( $1/r^3$ ) and that is known as near field. The transition zone linking the far and near fields somewhat is an undefined area [Mak2018].

6.1.4(a) Near Field Communication: There is no concrete near field communication formal definition. As per type of antenna and application it differs. The most common agreement lies in its definition wherein it is considered as lesser than by one wavelength ( $\lambda$ ) compare to the antenna. Wavelength in meters can be represented as  $\lambda = 300/f\text{MHz}$ . The most acknowledged distance of near field from the antenna is known as  $\lambda/2\pi = 0.159\lambda$ . The near-field coupling usage between RFID tag and reader may be expressed through magnetic induction principle of Faraday. When a RFID reader goes through a relatively larger alternating current via a coil, it results in a localized alternating magnetic field. However, if a RFID tag is positioned in this magnetic field which has a smaller coil, an alternating voltage appears across this magnetic field.

6.1.4(b) Far Field Communication: Just as the near field, during expansion of magnetic field, definition of the far field varies too. The variation of this field accounts from

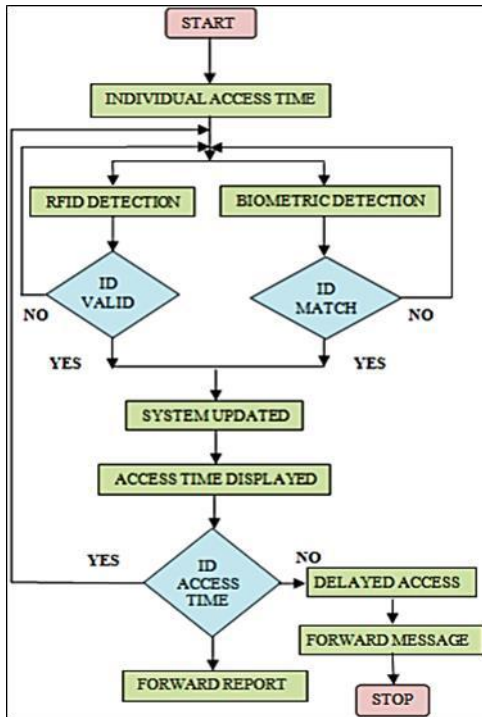
$2\lambda$  to  $3\lambda$  or even up to  $10\lambda$  from the RFID antenna. Another characterization of far field points out that it commences at  $5\lambda/2\pi$ , however some other descriptions indicate that it may be dependent on the biggest measurement of the antenna represented by  $D$  or  $50D^2/\lambda$ . The far field has been considered as the actual radio wave [Paa2015]. It propagates via space with speed of around 3 billion.



**Fig 3:** An Overview of Far and Near Field a RFID Antenna Design

## 2.4 RFID system workflow

The central database server operates in conjunction with the associated front-end RFID application which maintains the log in database and updates all the records of RFID tags. It also facilitates updating of user profiles in RAM of control circuit. User profile of an individual may include his/her personal details like Tag ID, name, date of birth, department name, phone number etc. The system can offer search profile with a query mechanism to support the tracking of individual in different circumstances [Qua2014].



**Fig 4:** Workflow Diagram of a Basic RFID System

There are many checks and balances provisioned in the system to ensure adequate security. As an example, it will prevent someone trying to access at two or more places at same instant with same tag ID. It can be further explained in a workflow illustration in figure 6.5 of a basic RFID system above. The processing of the proposed system is illustrated in the work flow in which it commences when the administrator exercises his/her option of login after the initiation of RFID reader.

RFID tag is detected by the reader the moment it comes within its range. Tag information in respect of the user is read by the RFID tag after referring it to the database [Liu2017]. Simultaneously, the biometric print of user is taken by the biometric device to authenticate the identity of a user to cross examine. In case the RFID Reader and biometric detections confirmed the match, system is updated and access time of user is displayed accordingly. However, in case of any mismatch of user identity with respect to RFID tag and biometric database, user has to go through the same exercise to verify his/her identity. During this ID authentication process, users' access time is recorded and a report is forwarded. But, if there is any delay to establish the users' ID, a message to be forwarded by the system. The RFID system can

convert any user institution with several user personals and departmental assets into a RFID enable campus. All the individual users and assets of that campus will be tagged with the unique Tag ID. These tags will be affixed in the users' smart identity cards. Different user departments will get tagged with unique RFID labels. The details of these tag IDs and labels will be stored in the RFID reader unit.

### **3. Results and Discussion**

#### **Promising future growth with an integrated UID solution**

A modern civilization which progressively relies on IoT based or online services need skills which can offer an individual and secure identity. It is an essential prerequisite for secure and an open ICT oriented civilization where public businesses services can flourish. Smart card technology in this regard has proven to be a perfect platform to horde such an individual identity. In many developed countries, roughly everyone carries microcontroller based secure security tokens or smart cards with them. Besides serving as an electronic ID, smart cards are also being utilized for micro purse, payment and functionality for transportation in a multi-application system gaining highest user acceptance [Zou2019]. They offer genuine user worth and a better degree of convenience. An illustration of current status of national identification schemes of various worldwide countries has been given in Fig 3 below which depicts their progress right from inception to roll out phases

#### **Current status of worldwide national IDs**

There are quite a few countries in the world which have either implemented or in the process of implementation of their national identity cards [Tia2018]. USA is still using their social security cards against their national identity cards. China too is using their second-generation ID. There are perception shortcomings against their prevalent ID which is considered as a digital intrusion by certain sections and challenge the legal rights of their citizens. Hong Cong is using its national identity card which includes minimum required data like name, Date of Birth (DOB), individual photo, residential address etc [Zou2018, Zon2019].



**Fig 5:** An Image of New National E-ID

After initial collection of user database and integrating it with national database, it had undergone through a rigorous and focused trial before adopting it as a national identity and now treated as one of the successful ID projects. South Africa too is in the process of implementation of their national ID by incorporating fingerprints as a means of biometric security.

### Conclusion

This research study has examined the evolution and necessity of human identification along with current worldwide scenario of existing national IDs. Integration of biometrics with smart card technology presents a strong authentication tool to the identity card holder. This research study offers an insight into the feasibility and technological aspects of this potential application. A recent trend of using Radio Frequency Identification (RFID) and biometric technologies for personal identification in e-passports and other applications too paves the way to explore a global identity solution. Currently, certain nations have mandatory ID cards system in their countries for their citizens and quite a few of them enforce to carry these IDs at all times. The technological proposition in this study of a universal ID system is a significant application in ongoing information technology evolutions. It is an evolution which compels worldwide governments to contemplate about distinctive identities for their citizens as an integrated entity [Zou2019]. A

single worldwide UID card for a global human mobility is yet to be accomplished and the proposed integrated identity solution with smart card based UID card along with RFID and a robust biometrics system does possess a potential to realize these expectations. The fundamental prerequisite with worldwide smart card and RFID applications have been studied in this research study which can present an ample platform in this proposal to absorb future technical upgrades for both associated hardware and software systems.

### **Future scope**

To further enhance this proposed system we can also develop a web interface where consumers can log in and check their past transactions. This system helps to keep track of ration content but the weighing of the content is still manual. To avoid human errors in the weighing of ration content we can add mechanical devices to automatically measure the ration content requested by the consumer.

### **References**

1. Badamasi YA. The working principle of an Arduino, in Electronics, Computer and Computation (ICECCO), 11th International Conference on Information Communication Embedded Systems, 2014, 1-4.
2. Yerlan Berdaliyev, Alex Pappachen James. RFID-Cloud Smart Cart System, IEEE Intl. Conference on Advances in Computing A Communications and Informatics (ICACCI), 2016, 21-24.
3. Vinayak T Shelar, Mahadev S Patil. RFID and GSM based Automatic Rationing System using LPC2148, International Journal of Advanced Research in Computer Engineering & Technology (IJARCET), 2015, 4(6).
4. Bichlien Hoang, Ashley Caudill. "RFID", IEEE Emerging Technology Portal, 2006-2012.
5. Anshu Prasad, Aparna Ghenge, Sonali Zende, Sashikala Mishra, Prashant Godakh. Smart Ration Card using RFID, Biometrics and SMS Gateway, IEEE International Conference on Inventive Communication and Computational Technologies (ICICCT), 2017.
6. Mohit Agarwal, Manish Sharma, Bhupendra Singh, Shantanu, Smart Ration Card using RFID and GSM, IEEE 5th International Conference-Confluence the Next Generation Information Technology Summit, 2014.

7. Bala Karthik K. Cloud-Based Ration Card System using RFID and GSM Technology, International Journal of Engineering Research & Technology (IJERT), 2013, 2(4).



**Chapter - 7**  
**Design Analysis of Ultra-Wide Band Micro Strip  
Patch Antenna**

**Authors**

**M.V.S. Sudheer Babu**

Assistant Professor, Department of ECE, Narayana Engineering  
College, Gudur, Andhra Pradesh, India

**M. Kondalu**

Professor, Department of EEE, Malla Reddy Engineering  
College, Hyderabad, Telangana, India

**Rajesh Reddy Duvvuru**

Assistant Professor, Department of EEE, Narayana Engineering  
College, Gudur, Andhra Pradesh, India



# Chapter - 7

## Design Analysis of Ultra-Wide Band Micro Strip Patch Antenna

M.V.S. Sudheer Babu, M. Kondalu and Rajesh Reddy Duvvuru

### Abstract

Antennas play a very significant role in wireless communication system as it converts the electrical signal (which propagates in the RF trans receiver) into electromagnetic waves (which propagate in the free space) successfully with minimum loss. Micro strip patch antenna is one of the most extensively used printed circuit antenna for today's world of mobile (or wireless) communication systems. Micro strip patch antenna comprises of a patch of radiating type on one side of the substrate's dielectric and a plane which is called a ground plane on the other side. Micro strip antennas are in demand because it has many striking features like planar configuration, light weight, low profile, reduced cost, light weight and conformability

**Keywords:** MS

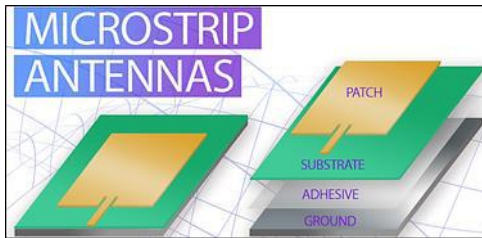
### 1. Introduction

The definition of antenna or aerial according is simply “a metallic device for radiating or receiving radio waves”. Basically an antenna can be considered as a connecting link between free-space and transmitter or receiver Microstrip antennas (MSAs) are one of the important classes because of its different application in microwave communication. The novel design and development of microwave antennas are the most important task in microwave communication systems which achieve the desired radiation requirements. The technology of microstrip antenna is a developing topic in the field of antenna and creating interest among industrialists, academicians, professional engineers and researchers throughout the world [2]. The configuration of microstrip antenna (MSA) is planar and has the advantages of printed circuit technology. The radiating patch of MSA is etched with copper or gold photo on one side, which has dielectric substrate board, on the other side of the board consisting of metallic ground plane [3]. G.A. Deschamps [4] first proposed the concept of the MSA in 1953. Robert E.

Munson [5] and John Q. Howell [6] developed the practical antennas in the later 1970s. The MSA radiating patch is of any geometry viz; square, triangular, rectangular, circular, elliptical, sectoral, annular ring etc. The commonly used MSA is rectangular microstrip antenna because of the simplicity in design, fabrication and ease of analysis.

The technology like ultra-wideband is like a structure that has covered almost 500 MHz of bandwidth or covers a fraction bandwidth of either 20% or greater than that. Depending upon the micro strip antenna's point of view, ultra wideband technology almost occupies presently three important types of applications

- a) Modern ultra-wide band operates in 3.1 to 10.6 GHz frequency band.
- b) Signal intelligence and detection.
- c) Ground Penetrating Radars (1MHz to 10 GHz).



**Fig 1:** Micro Strip Antenna view

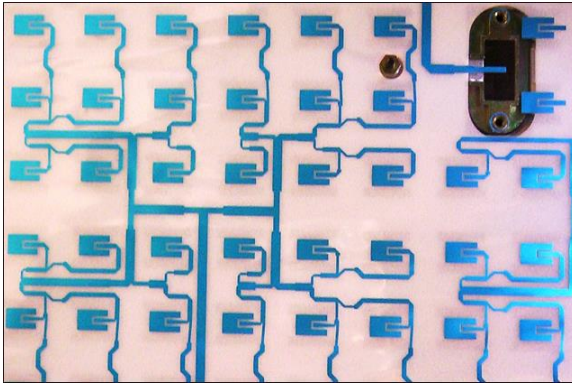
An Ultra-Wideband technology is referred as a system which covered over 500 MHz of bandwidth or covers a fractional bandwidth of either 20% or greater than that. Basically, ultra wideband applies a method or technique of radio modulation to attain a broad bandwidth by broadcasting very short type pulses which may be in nanosecond or less with very minimum utilization of power. So, ultra-wideband technique using radio modulation is different from the narrow band conventional type of communication systems. Micro strip antenna with suitable patch is very common and widely used in telecommunication because of their low-profile structure the conventional micro strip patch antenna has a narrow band properties, wide beam micro strip patch antenna uses different techniques for attaining wide band. The wide bandwidth of micro strip antenna is achieved by using defected ground or defected micro strip technologies. In these technologies, the fabrication is done by etching the antenna element either on the metal part of the antenna patch, place on the insulating dielectric substrate or the ground plane which is a continuous metal layer on the opposite side of the

dielectric substrate. The two cheaper fabrication technologies are press machining and photo etching. These technologies have actually made the printed antenna technique appropriate for low priced manufacturing in the productions which is in large scale. Now a day, integrated wireless applications of digital type are very much in demand by the user. The low-profile wide band type, low volume, low cost and light weight antennas are suitable for these types of applications So, micro strip antenna is fit and is preferred for meeting these types of requirements

## **2. Micro strip antenna design**

Micro strip radiating patch components are a kind of antenna having resonant type behaviour and these antennas can carry various resonating patterns. Whenever, the micro strip resonant patch antenna is planned at the basic fundamental pattern, patch size is minimum but the impedance bandwidth that is attained has ultra wide band or narrow band. In UWB, it has no practical use for communication due to addition of noise and for narrow band generally not sufficient to disguise the operational frequencies of latest applications of wireless communicating structures or applications. A number of schemes to increase the bandwidth of micro strip patch antenna have been suggested for enhancing the efficiency of the wave-signal transmission through the proposed antenna, the following contributions are implemented in the present works as follows:

The convex type conformal antenna is presented with the rectangular SIW. •The irregular rectangular patch resembling two definite L shapes are placed •along with the circular patches at top and bottom position of those L shapes the presented design was then simulated for the radiation pattern and return •loss curve. The proposed conformal antenna array is depicted in figure. 2. The antenna loses its high directivity property and the steering direction of the original rectilinear design. Using the above theory, conformal antenna is presented which provides beams in broadband direction. The SIW can be equivalent to the conventional rectangular waveguide, where the periodic metallic circles in SIW are considered as the sidewall of the conventional waveguide. Therefore, the SIW with irrational rectangle-shaped slots is presented. The conformal micro strip LWA is also developed which composed of a metallic strip over a dielectric substrate with a ground plane. A single feed port is placed on the edge of the antenna by feed patch to serve, as a travelling wave transmission line.



**Fig 2:** Micro Strip Antenna Design

**Antenna Design Specifications** The three important parameters in the design of Micro strip Patch Antenna's are: Frequency of operation ( $f_r$ ): The selection of appropriate resonant frequency for the micro strip patch antenna should be chosen for a particular application. Dielectric constant of substrate material ( $\epsilon_r$ ): The size of the micro strip antenna can be minimized by selecting a dielectric substrate with a very high dielectric constant. Height of dielectric substrate ( $h$ ): For the micro strip patch antenna to be utilized in various sensitive wireless devices like cellular phones, so it is necessary that the antenna used in that device is not bulky.

### 3. Proposed antenna with DGS and DMS

Now on the basis defected ground structure and defected micro strip theory, two symmetrical slots have been etched at the patch, i.e. the defected micro strip structure (DMS) to disturb the current and the defected ground structure (DGS) at the ground under feed line to create stop band. The proposed antenna with DGS and DMS is shown in Figure.

**Table 1:** Dimensions of the proposed antenna

Parameter/Dimensions	Description	Value in mm
These are the same dimensions that have been used for the reference antenna	L	31
	L2	11
	L3	14.85
	W	20
	W1	1.525
	W2	10.45
Length of symmetrical slots on patch (DMS)	$L_{pslot}$	10mm
Width of symmetrical slots on patch (DMS)	$W_{pslot}$	2mm

Length of symmetrical slots on ground (DGS)	$L_{gs\text{slot}}$	4.8mm
Width of symmetrical slots on ground (DGS)	$W_{gs\text{slot}}$	2.3mm
Feeding Technique-Micro strip feed		

The parameters or dimensions of the proposed antenna with description and values in mm are shown in the table above. The dimensions of parameters of the proposed antenna from front and back side are same as for reference antenna but the difference lies in the technology of the DGS and DMS which has been used in the ground plane and in the patch of proposed antenna. The various dimensions of slots which are symmetrical in nature and is etched on the lower ground plane and the upper patch with different values of length and width that have been revealed in the above table. The patch of the proposed micro strip has also been excited by the micro strip feed line.

#### 4. Results and Discussion

The performance of the designed antenna is analyzed using HFSS computer design and simulation tool. The simulation results are included in this section. In figure. 3, input reflection coefficient, S11 is getting a maximum point at 14.5 GHz, with -50.15 dB magnitude. It is behaving as a resonant antenna in Ku band at 14.5 GHz.

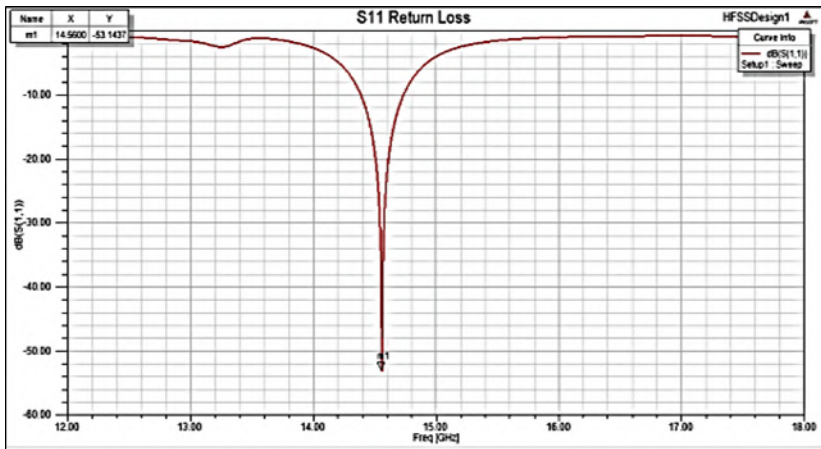
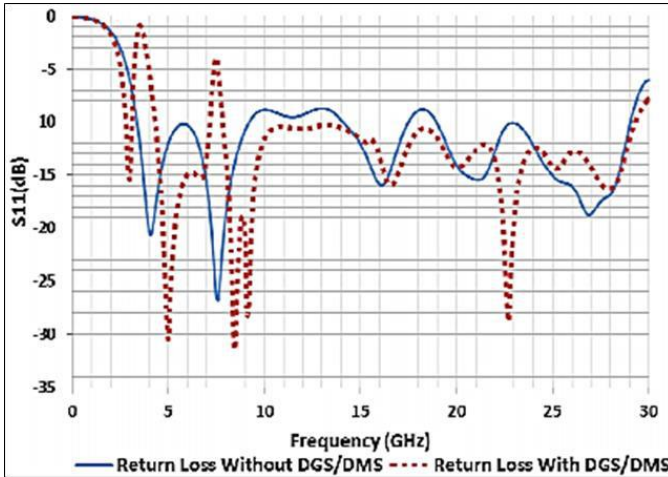


Fig 3: Reflection coefficients for the conformal antenna

The results of the proposed and the conventional micro strip antenna in terms of resonant frequencies and bandwidth from the return loss graph are given below. Return loss shows the total power amount that has been vanished to load and is not returned as reflection. Basically the parameter return loss is similar to VSWR (Voltage standing wave ratio) which specifies

how good the matching is done between micro strip antenna and communication transmitter. Perfect value of return loss is around -10dB which relates to VSWR of less than 2. The Return Loss graph of proposed and reference micro strip antenna is revealed in Figure.



**Fig 4:** Return loss vs frequency

The plot of S11 in dB versus the frequency in GHz of the antenna without DGS and DMS technology in blue colour graph and with DGS and DMS technology in red colour graph has been plotted in figure. The S11 parameter is also known for the return loss of antenna. The design micro strip antenna is of notched type and is used for ultra-wide band applications which work on the multi-band operations. As the values of the frequency increases, various bands have been seen on the graph. It is observed from the graph that the proposed antenna works for multi bands as compared to reference antenna.

Various values of resonant frequencies for the proposed antenna are at 22.65 GHz, 9.1 GHz, 8.4 GHz, 5 GHz and 2.9 GHz. And the bandwidth for different bands is different and can be used for ultra-wide band-based applications. The graph between S11 dB and the frequency is used for measuring the bandwidth of the micro strip antenna at the value -10dB. At this value, the difference between two frequencies of the valid band can be measured which is known as band width of that particular band.



**Table 2:** Important parameters for the proposed antenna

Resonance Frequencies (GHz)	Max Gain (dB)	Gain (dB) at Phi=0, Theta =0	Gain (dB) at Phi=0, Theta =90	Gain (dB) at Phi=90, Theta =0	Gain (dB) at Phi=90, Theta =90
2.9	1.002	1.002	1.002	1.002	-28
5	3.6	3.6	3.6	3.6	-23
8.4	4.7	4.13	-4	4.1354	-21
9.1	3.2	2.9	-3	2.7	-20
22.65	5.6 (at elevation angle 14.8°, 78°, 160°)	-2	4	-2	-3

## Conclusion

The results of the experimental investigations and theoretical validations are described in the present chapters. In this chapter, the conclusions drawn from those extensive results are summarized. The future scopes for carrying out further investigations related to the work are also reported. In the radiating element of CRMSA the various shaped slots are designed and incorporated to get wider impedance bandwidth. The possible study is conducted by loading rectangular slot in the patch. The slot is varied in terms of location and dimension to obtain multiband and broadband operation. The vertically five open stub RMSA (VOSRMA) is constructed which gives hexa band operation as shown in above figures with maximum impedance bandwidths of 8.37% at middle band of frequencies and gives maximum gain of 2.35 Db.

## References

1. Cao W, Chen ZN, Chen W, Chen, Zhang B, Liu A. A beam scanning leaky-wave slot antenna with enhanced scanning angle range and flat gain characteristic using composite phase-shifting transmission line, IEEE Transactions on Antennas and Propagation. 2014; 62:5871-5875.
2. Chen J, Zhang Q. High Scanning-Rate Periodic Leak-Wave Antennas using Complementary Microstrip Slotline Stubs, in proceedings of sixth Asia-Pacific Conference on Antennas and Propagation (APCAP), 2017, 1-3.
3. Chen J, Zhang Q. Scanning-Rate Enhancement of Periodic Leak-Wave Antennas using Delay Element, in proceedings of International Conference on Microwave Millimeter Wave Technology, 2018, 1-3.

4. Chiu L, Hong W, Kuai Z. Substrate integrated waveguide slot array antenna with enhanced scanning range for automotive application, in proceedings of APMC 2009-Asia Pacific Microwave Conference, 2009, 1-4.
5. Guan DF, Zhang Q, You P, Yang ZB, Zhou Y, Yong SW. Scanning Rate Enhancement of Leaky Wave Antennas using Slow-Wave Substrate Integrated Waveguide Structure, IEEE Transaction Antennas Propagation. 2018; 66:3747-3751.
6. Guglielmi M, Jackson DR. Broadside radiation from periodic leaky-wave antennas, IEEE Transactions on Antennas and Propagation. 1993; 41:31-37.
7. Haghighi SS, Heidari A, Movahhedi M. A Three-Band Substrate Integrated Waveguide Leaky-Wave Antenna Based on Composite Right/Left-Handed Structure, IEEE Transactions on Antennas and Propagation. 2015; 6:4578-4582.